Student thesis series INES nr 777

Effects of ecosystem integrity on drought resistance and recovery of forests on a global scale

Pengfu Yao

2026

Department of

Earth and Environmental Sciences

Lund University

Sölvegatan 12

S-223 62 Lund

Pengfu Yao (2026).

Effects of ecosystem integrity on drought resistance and recovery of forests on a global scale

Master degree thesis, 30 credits in *GIS and Remote Sensing*
Department of Earth and Environmental Sciences, Lund University

Level: Master of Science (MSc)

Course duration: *January* 2026 until *June* 2026

Disclaimer

Effects of ecosystem integrity on drought resistance and recovery of forests on a global scale

---

Pengfu Yao

Master thesis, 30 credits, in *GIS and Remote Sensing*

Supervisor: Lanhui Wang

Department of Earth and Environmental Sciences, Lund University

Examiner: Cecilia Akselsson

Department of Earth and Environmental Sciences, Lund University

Acknowledgement

I would like to express my sincere gratitude to my supervisor, Lanhui Wang, for his patient guidance throughout my project, which allowed me to learn a great deal. I would also like to thank my project examiner, Cecilia Akselsson, for attending my seminar.

I would like to express my appreciation to my friends and family for their support and encouragement during difficult times, whether they were by my side or not.

Abstract

Droughts are intensifying under climate change and increasingly threaten the carbon and water functions of global forests, yet the factors that determine forest resilience to drought remain debated. Resistance—the capacity to withstand a drought—and recovery—the capacity to return to pre-drought function—are two complementary components of resilience that may be shaped differently by forest integrity. How its landscape-level and species-level dimensions act on each component, and whether they trade off against one another, has not been quantified globally. Using monthly satellite-based solar-induced chlorophyll fluorescence and 3-month Standardized Precipitation Evapotranspiration Index–based drought events from 2001 to 2022, we calculated pixel-level resistance and recovery for 611,540 stable forest pixels at 0.05° resolution. Two dimensions of forest integrity—landscape-level integrity (Forest Landscape Integrity Index, FLII) and species-level integrity (tree species diversity)—were modelled against resistance and recovery using Random Forests, and against the resistance–recovery trade-off using a boosted regression tree, controlling for climate, soil, topography, and baseline forest structure. Tropical forests showed higher resistance but lower recovery, while boreal and temperate forests showed the opposite, and a negative event-level resistance–recovery correlation was observed in 72.98% of pixels. Tree species diversity was positively associated with resistance but negatively with recovery, with its effects modified by temperature and precipitation. FLII contributed less strongly, likely reflecting shared variance with tree cover and a scale mismatch between landscape-level processes and coarse pixel-level responses. These results suggest that no single dimension can capture forest integrity, and that resistance and recovery are complementary yet not interchangeable components of forest drought resilience.

Keywords: Geographical Information Science, Drought resilience, Forest landscape integrity, GOSIF, Resistance–recovery trade-off, SHAP, SPEI, Tree species diversity

Table of Contents

1. Introduction

1.1 Drought, climate change, and the future of global forests

Drought is one of the most widespread climatic stresses on forest ecosystems, and under ongoing climate change, it is expected to become more frequent, more severe, and more spatially extensive (Allen et al., 2010; Xu et al., 2019). Forests are highly sensitive to water deficit because their growth, photosynthesis, carbon uptake, and survival all depend on water availability. Severe drought reduces vegetation productivity, increases tree mortality, and alters ecosystem structure, and these impacts are projected to intensify under future climate (Xu et al., 2019). Recent satellite analyses also suggest that many forest biomes are already losing resilience to climatic stress (Forzieri et al., 2022). Because forests regulate the global carbon cycle and provide a wide range of ecosystem services, these changes have implications well beyond local ecology.

A second concern is that most of the world's forests are no longer in a natural state. Logging, road building, agricultural expansion, and the indirect pressures of fragmentation and edge formation have left the majority of the remaining forest area in a modified condition (Grantham et al., 2020). Whether and how this human modification weakens the ability of forests to cope with droughts has not been quantified at the global scale. This thesis addresses that gap.

1.2 Drought resistance and recovery of forests

Forests do not respond to drought in the same way everywhere. Some forests show only minor functional losses during drought, while others experience large declines in productivity. Some recover within months, while others remain suppressed for years (Schwalm et al., 2017; Sturm et al., 2022). These spatial differences imply that drought impacts cannot be understood solely from drought intensity; they also depend on ecosystem properties that determine how forests respond.

To capture this variation, ecosystem resilience is used here as the umbrella concept, with two complementary, measurable dimensions: resistance and recovery (Hodgson et al., 2015; Ingrisch & Bahn, 2018). Resistance describes the ability of an ecosystem to maintain function during drought. Recovery describes how quickly function returns after drought ends. Both can now be quantified globally from satellite vegetation data (Runge et al., 2025).

The distinction matters because high resistance does not always imply high recovery. A repeated finding is that the two are inversely related: forests that resist drought well tend to recover more slowly, and vice versa (Yao et al., 2024). This trade-off limits the long-term resilience and stability of forest function under repeated droughts. When the trade-off is weak, forests can combine both properties, resulting in higher overall resilience and stability.

1.3 Forest ecosystem integrity at two levels

Beyond climate and site conditions, the integrity of a forest itself is expected to shape its response to drought. In this thesis, forest integrity is considered at two complementary levels. Landscape-level integrity is represented by the Forest Landscape Integrity Index (FLII), which measures the degree to which a forest has been modified by human pressures (Grantham et al., 2020). Species-level integrity is represented by tree species diversity, which reflects the variety of tree species present and the resulting breadth of functional strategies for coping with drought (Anderegg et al., 2018; Liu et al., 2022).

FLII is a globally consistent, continuous index of forest condition that combines observed human pressures, inferred indirect effects, and loss of forest connectivity into a single score from 0 (most modified) to 10 (least modified) (Grantham et al., 2020). Only about 40% of the world's remaining forests are considered to have high integrity. Forests with high FLII scores tend to have larger interior area, lower edge exposure, and stronger connectivity—properties that can buffer microclimate and reduce the drying effects of fragmentation (De Frenne et al., 2019; Haddad et al., 2015).

Tree species diversity provides a complementary indicator. Forests with more tree species contain a wider range of drought-response strategies, including variation in rooting depth, stomatal regulation, and hydraulic traits. When some species are strongly affected by drought, others may continue to function, helping the community as a whole maintain productivity (Anderegg et al., 2018). At the global scale, species diversity has been shown to enhance drought resistance across a large fraction of the world's forests (Liu et al., 2022).

These two dimensions are related but not equivalent. High FLII does not always imply high species diversity, and species-rich forests can still be fragmented or edge-exposed. Whether each dimension independently predicts drought resilience, after accounting for climate, soil, and topography, has not been tested at the global scale. The mechanisms behind each are reviewed in detail in Chapter 2.

1.4 Research gap

Despite these mechanisms, an important knowledge gap remains. Global studies of forest drought resilience have mostly focused on climate, biome type, soil, topography, or baseline vegetation conditions. These factors are clearly important, but they do not capture the role of forest integrity. Work on landscape integrity has emphasised biodiversity conservation, habitat quality, and carbon storage rather than drought resilience (Watson et al., 2018). Although global-scale evidence on the diversity–drought link is beginning to emerge (Liu et al., 2022), most studies still examine diversity in isolation, without considering the landscape context (Anderegg et al., 2018; Bai & Tang, 2024). Existing work on either dimension tends to focus on single mechanisms, single biomes, or single drought events, and rarely separates the integrity signal from the strong climate gradients that drive both human pressure and forest function (Su et al., 2025).

As a result, several questions remain open. First, it is unclear whether FLII and tree species diversity are independent predictors of drought resilience after accounting for climate, soil, topography, and forest tree cover. Second, the relative importance of landscape-level versus species-level integrity has not been compared in a single analytical framework. Third, it is not known whether the effects of these two dimensions vary across major environmental controls. This gap matters because forest conservation and restoration are increasingly promoted as nature-based solutions to climate change, and their effectiveness in supporting drought resilience requires quantitative evidence that accounts for both landscape conditions and species composition.

1.5 Research aims and hypotheses

This thesis aims to test, at the global pixel level, whether FLII and tree species diversity are independent predictors of drought resilience in forest ecosystems, after controlling for climate, soil, topography, and baseline forest structure (here represented by tree cover, i.e., the mean percent tree cover over the study period). The analysis focuses on stable forest pixels in order to reduce the influence of land-cover change, deforestation, and forest gain during the study period.

The study uses 22 years of monthly solar-induced chlorophyll fluorescence (SIF) from the GOSIF v2 product (2001–2022) as a proxy for forest productivity. SIF is preferred over reflectance-based vegetation indices because it tracks photosynthetic activity directly and responds to drought stress earlier and more sensitively. Drought events are identified from the

3-month Standardized Precipitation Evapotranspiration Index (SPEI-3). For each event in each pixel, resistance (Rt) and recovery (Rc) are computed from detrended SIF anomalies, and pixel-level median values are then linked to FLII, tree species diversity, and other environmental covariates using machine-learning models.

Two hypotheses are tested:

H1: After controlling for climate, soil, topography, and baseline forest structure, forests with higher FLII show greater drought resistance and faster drought recovery than forests with lower FLII.

H2: After the same controls, forests with higher tree species diversity show greater drought resistance and faster drought recovery than forests with lower diversity.

As a complementary analysis, the pixel-level drought resistance–recovery trade-off is examined to assess whether forest integrity is associated not only with the two dimensions of resilience individually but also with the temporal relationship between them.

2. Literature Review

This chapter reviews the literature that motivates the hypotheses tested in this thesis. Section 2.1 documents how climate change is reshaping forest exposure to drought. Section 2.2 introduces the conceptual framework of ecological stability and clarifies how resistance, recovery, and resilience are used in this context. Section 2.3 reviews how these concepts have been operationalised with remote sensing, including the choice of SIF over reflectance-based vegetation indices. Section 2.4 covers the resistance–recovery trade-off. Section 2.5 reviews the mechanisms through which landscape-level and species-level forest integrity are expected to influence drought resilience.

2.1 Drought and forest ecosystems under climate change

Drought is the most spatially extensive climatic extreme, and its impact on forests has become a central concern in global ecology. Allen et al. (2010) compiled the first global synthesis of drought- and heat-induced tree mortality, documenting episodes on every forested continent and identifying climate-driven physiological stress as the dominant cause. Their review made clear that mortality was not confined to arid systems: even mesic forests could collapse under unprecedented combinations of low precipitation and high temperature. Xu et al. (2019) extended this picture with 13 Earth system models, showing that the frequency of extreme

droughts will rise faster than that of mild or moderate droughts during the twenty-first century, and that the global reduction in gross primary productivity (GPP) caused by extreme droughts is projected to nearly triple by the end of the century relative to the 1850–1999 baseline.

These shifts have already begun to leave a measurable signature on forest carbon dynamics. Hubau et al. (2020) reported that the carbon sink in intact tropical forests has been declining for decades in Amazonia and is now beginning to weaken in Central Africa, driven by rising temperatures, increasing drought severity, and accelerating tree mortality. At the global scale, Forzieri et al. (2022) used satellite time series to show that critical-slowing-down indicators of resilience are declining in tropical, arid, and temperate forests over 2000–2020, while boreal forests show divergent local trends; they attributed these declines to elevated water limitation and increased climatic variability. Schwalm et al. (2017) added that the time required for ecosystems to recover from drought is itself increasing, and that recovery duration is now long enough in many regions that consecutive droughts can prevent full return to pre-drought function.

Together, these studies converge on three messages that frame the present study. First, drought is no longer a regional issue: it shapes carbon, biodiversity, and ecosystem-service outcomes across most forest biomes. Second, the response of forests to drought is variable in space and time, which makes it tractable for empirical modelling. Third, declines in resilience are already detectable from satellite records, which means it is now possible — and necessary — to ask which forest characteristics predict whether a given location will resist or recover well from a drought event.

2.2 Conceptual frameworks of ecosystem resilience to drought

The vocabulary used to describe how ecosystems respond to disturbance is older than the satellite era but has been repeatedly refined for empirical use. Pimm (1984) reviewed the early stability literature and showed that the term *stability* had been used to refer to at least five distinct properties, including resistance to perturbation and the rate of return to equilibrium. He argued that progress required treating these as separate, measurable quantities rather than a single concept. Hodgson, McDonald, and Hosken (2015) made the same point more recently, proposing that resilience should be decomposed into two complementary, jointly measurable components: resistance, the capacity to maintain function during disturbance, and recovery, the capacity to return to pre-disturbance function afterwards. This decomposition has since become the standard framework for empirical resilience studies in ecology.

Hillebrand et al. (2018) extended this framework with experimental data and showed that resistance, recovery, and temporal stability are independent dimensions: a system can score high on one and low on another, and no single metric captures the full response of an ecosystem to a disturbance. They concluded that any analysis of ecological stability should clearly report at least two of these dimensions. Ingrisch and Bahn (2018) reviewed the diverse metrics used in the field and modelling literature and proposed a normalized, bivariate framework in which resistance (the magnitude of the impact) and recovery rate (the speed of return) are reported on comparable axes. Their framework has been widely adopted and underlies many of the satellite-based applications discussed in the next section.

The terminology used in this thesis follows directly from this body of work. Drought resilience is the umbrella concept. Resistance (Rt) and recovery (Rc) are its two measurable dimensions, and they are computed separately for every forest pixel. This wording avoids the ambiguity criticised by Pimm (1984), Hodgson et al. (2015), and Ingrisch and Bahn (2018), and aligns with the framework adopted in the global remote-sensing studies reviewed below.

2.3 Quantifying ecosystem drought resistance and recovery from remote sensing

Translating resistance and recovery from concepts into measurable global quantities required three components: a method to detect drought events, a method to track vegetation function continuously, and a procedure to attribute changes in function to drought rather than to other variability. Lloret, Keeling, and Sala (2011) provided the foundational measurement framework in a tree-ring study of ponderosa pine. They proposed that resistance be computed as the ratio of growth during drought to pre-drought growth, and that recovery be computed as the ratio of post-drought growth to growth during drought. Although the original formulation was based on annual ring widths, the same logic — pre-disturbance baseline, disturbance minimum, post-disturbance return — has since been ported to remote-sensing applications almost unchanged.

De Keersmaecker et al. (2015) were among the first to apply this logic at the global scale using satellite data. Working with monthly NDVI from 1981 to 2011 and the Standardized Precipitation Evapotranspiration Index (SPEI; Vicente-Serrano, Beguería, & López-Moreno, 2010), they built a regression-based model of how vegetation anomalies respond to short-term climate anomalies and derived global maps of resistance and resilience. Their work demonstrated that the Lloret-style decomposition could be implemented at a quasi-global scale

and that the resulting metrics were spatially structured by biome, climate, and vegetation cover. Schwalm et al. (2017) brought a complementary perspective to the recovery side of the problem: using three independent estimates of GPP, they computed how long ecosystems took to return to their pre-drought state and showed that recovery time was longest in the tropics and at high northern latitudes, that more severe and longer droughts produced longer recoveries, and that the global area of ecosystems undergoing active recovery had grown over the twentieth century. Sturm et al. (2022) showed that the same framework could be applied at a much finer resolution. Using more than one million 10-m forest pixels from Sentinel-2, they quantified resistance, recovery, and resilience to the 2018 Central European drought and showed that Swiss forest responses varied systematically with topography, stand structure, and dominant species.

Yao et al. (2024) extended these methods to three decades of LAI data and showed that the spatial patterns of resistance and resilience are not stationary: the long-term correlation between the two has changed in recent decades, indicating that the global organisation of forest resilience and stability is itself evolving. Their methodology and findings provide a key reference point for the present study, both as a baseline against which the current trade-off measure can be compared and as an example of how mismatches between the chosen vegetation index and the underlying ecological process can shape conclusions.

This last point motivates an important methodological choice in this thesis: SIF is used in place of reflectance-based vegetation indices such as NDVI or EVI. Sun et al. (2015) demonstrated, using GOME-2 SIF observations of two contrasting U.S. droughts, that satellite SIF tracks both structural and physiological responses to drought through changes in absorbed PAR and fluorescence yield, and that SIF anomalies are correlated with root-zone soil-moisture anomalies. Behera et al. (2025) extended this evidence by showing that SIF yield can detect emerging drought stress one to two months before standard hydrological and meteorological indicators. The GOSIF v2 product of Li and Xiao (2019), which combines OCO-2 SIF retrievals with MODIS reflectance and MERRA-2 meteorology, makes these advantages available at 0.05° resolution, 8-day intervals, and global coverage from 2000 onwards. Together, these studies establish that SIF responds to drought stress earlier and more sensitively than greenness indices and that GOSIF is the appropriate global product for the pixel-level, event-based analysis pursued here.

2.4 The drought resistance–recovery trade-off

The idea that resistance and recovery may not be jointly maximisable has been part of the stability literature since at least Pimm (1984). The empirical question of whether such a trade-off exists across global ecosystems was addressed directly by Yao et al. (2024). Using GIMMS LAI data over three decades, they computed pixel-level resistance and resilience and reported a globally significant negative correlation between the two — that is, ecosystems that resisted drought well tended to recover more slowly. They also showed that the strength of this trade-off has weakened over time, with the proportion of pixels showing both low resistance and low recovery (the worst combination) increasing.

Two methodological points motivate a small extension introduced in this thesis. First, both Yao et al. (2024) and Bai and Tang (2024) computed the trade-off as a spatial correlation across pixels or sites. This approach captures whether locations with high resistance tend to differ from those with high recovery, but it does not quite answer whether a single forest patch repeatedly behaves in a high-resistance, low-recovery (or low-resistance, high-recovery) manner across multiple drought events. The latter is closer to the original ecological notion that resistance and recovery are competing strategies of the same ecosystem. Second, the strength of the trade-off varies systematically across environments. Wu and Liu (2025), for example, reported that the resistance–resilience trade-off in northern ecosystems weakens with altitude, suggesting that high-altitude forests activate multiple stabilisation mechanisms simultaneously. Whether forest integrity exerts a similar moderating influence has not yet been tested.

2.5 Forest integrity as a driver of forest drought resilience

Landscape-level integrity (FLII)

Grantham et al. (2020) introduced FLII as a globally consistent, continuous index that integrates three components: observed human pressures (e.g., infrastructure, agriculture, and recent deforestation), inferred indirect pressures radiating from those observed pressures (e.g., access-driven extraction), and loss of forest connectivity. The resulting score ranges from 0 (most modified) to 10 (least modified) at roughly 300-m resolution. Their global mapping showed that only about 40% of the remaining forest area has high integrity, with high-integrity forests concentrated in the boreal regions of Russia and Canada and in the major tropical blocks of the Amazon, the Congo Basin, and New Guinea. Watson et al. (2018) had earlier argued, in a synthesis of conservation evidence, that intact forests provide disproportionately greater amounts of biodiversity, carbon storage, water provision, and other ecosystem services than

structurally similar but degraded forests. FLII has since been adopted as a complementary indicator within the Kunming-Montreal Global Biodiversity Framework and is now widely used as a standardized proxy for forest condition.

Several mechanisms link landscape-level integrity to drought resilience. First, intact forests maintain closed canopies that buffer understorey conditions. De Frenne et al. (2019) showed across 98 sites on five continents that closed forest canopies cool the understorey maximum temperature by an average of 4.1 °C and warm the minimum by about 1 °C, with the strongest buffering under the most extreme ambient conditions. This microclimate regulation can reduce drought stress on trees and understorey vegetation. Second, forests with low integrity are often fragmented and edge-exposed. Haddad et al. (2015) reported that 70% of remaining forest worldwide lies within 1 km of a non-forest edge; Banbury, Morgan and Jucker (2025) showed that edge forests are systematically warmer, drier, and more wind-exposed; and Koelemeijer et al. (2023) demonstrated that edge effects on understorey growth were nearly twice as strong during the 2018 European drought as during non-drought years. Third, landscape fragmentation directly affects forest resilience. Using global tree-cover data and three independent fragmentation metrics, Su et al. (2025) found a significant fragmentation–resilience relationship in about 77% of fragmented forests, with the effect direction varying by biome—negative in tropical and temperate forests but positive in boreal forests.

Species-level integrity (tree species diversity)

The central idea is that forests with more tree species exhibit a wider range of functional traits related to drought response, including differences in rooting depth, stomatal behaviour, wood density, and hydraulic architecture. When drought occurs, species with different strategies are affected to different degrees, so the overall community maintains higher productivity than a low-diversity community in which most individuals respond similarly.

This idea has strong empirical support. Isbell et al. (2015) showed across 46 grassland experiments that high-diversity communities lost roughly half as much productivity during climate extremes as low-diversity communities. Anderegg et al. (2018) extended this finding to forests: using data from 40 flux-tower sites, they found that hydraulic-trait diversity was the strongest cross-site predictor of drought response, more important than mean trait values or species richness alone. At the global scale, Liu et al. (2022) reported that species diversity enhances drought resistance in roughly half of the world's forests, based on more than 700,000 forest plots. Most recently, Bai and Tang (2024) confirmed the diversity effect using tree-ring

records from 4,072 sites and showed that species-rich forests exhibit a weaker resistance–recovery trade-off, suggesting that diversity may help forests maintain both resistance and recovery simultaneously.

Why are both dimensions needed? Landscape integrity and species diversity are correlated but not interchangeable. Intact forests tend to retain higher species diversity because the same human pressures that fragment landscapes and create edges — logging, road building, agricultural expansion — also reduce species richness over time. However, the two dimensions capture different aspects of forest condition. FLII reflects the physical and spatial structure of the forest landscape, including connectivity, edge exposure, and the intensity of surrounding land use. Tree species diversity reflects the ecological composition of the forest community and its potential for functional complementarity under stress. A highly connected forest with low species diversity may lack the functional breadth to cope with drought, whereas a species-rich forest fragment may still suffer from edge drying and exposure to microclimate conditions. Whether each dimension contributes independently to drought resilience, after accounting for the effects of climate, soil, and topography, is the central question of this thesis.

3. Methods

3.1 Study design

This study assesses how forest integrity affects ecosystem responses to drought at the global scale. Forest integrity is represented by two variables: the Forest Landscape Integrity Index (FLII) at the landscape level, and tree species diversity at the species level. The analysis covers stable forest pixels from 2001 to 2022 — only pixels with valid vegetation activity, drought information, stable forest cover, and complete predictor values are retained.

The workflow has four steps (Figure 1): (1) preprocessing monthly ecosystem productivity, drought data, forest cover, forest integrity indicators, and environmental predictors to a common 0.05° grid; (2) detecting drought events from SPEI-3 and computing pixel-level resistance (Rt) and recovery (Rc) from detrended SIF anomalies; (3) constructing a common model table with collinearity screening and target transformation; and (4) fitting Random Forest models for resistance and recovery and a boosted regression tree (BRT) model for the resistance–recovery trade-off. The detailed methods are described in Sections 3.2–3.6.

The resilience metrics are drought resistance, drought recovery, and the resistance–recovery trade-off. Resistance describes the ability of ecosystem productivity to resist decline during drought. Recovery describes the ability of ecosystem productivity to return to normal after a drought-induced decline in productivity. The trade-off is represented by the event-level correlation between resistance and recovery within each pixel.

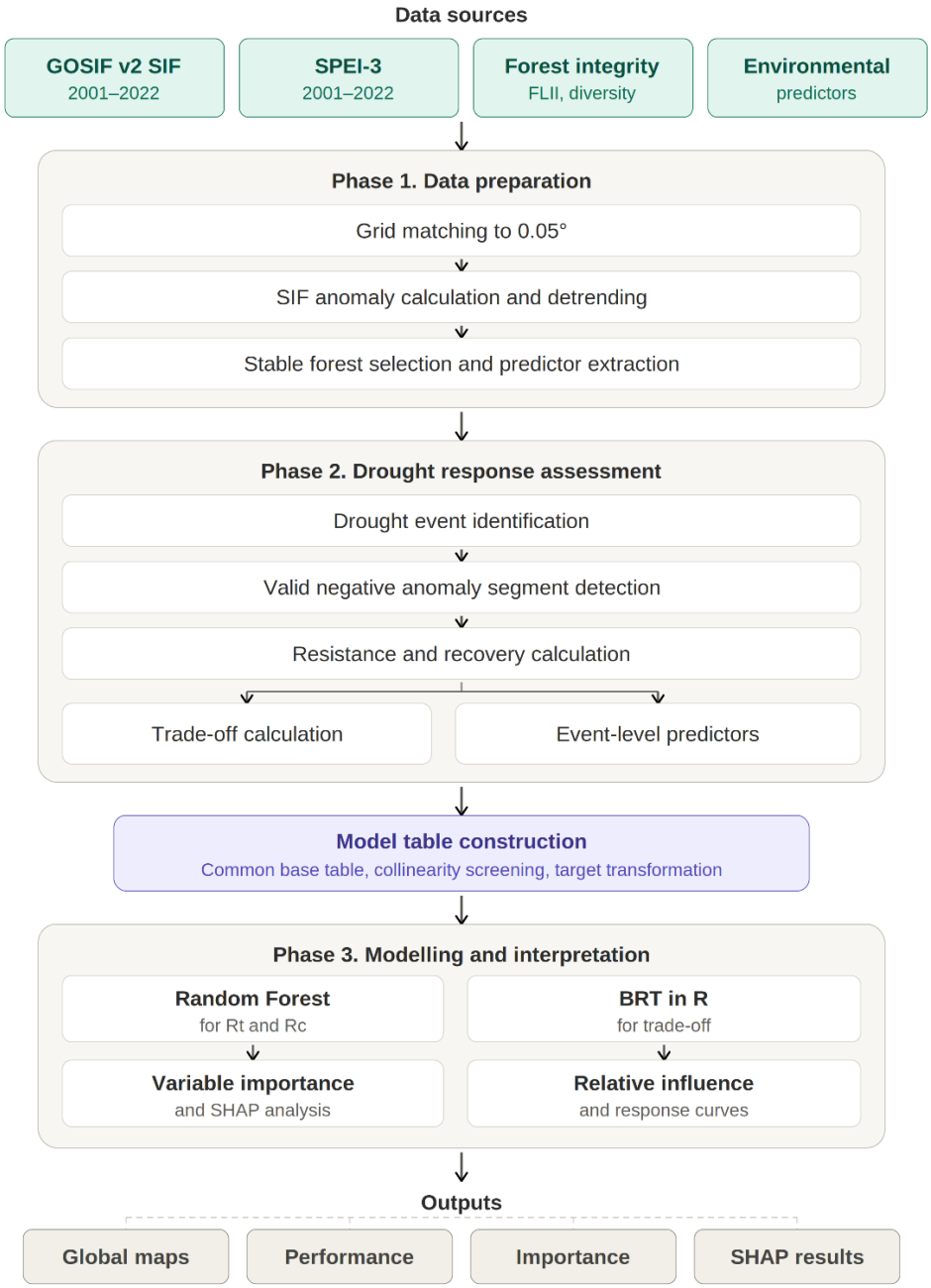

Figure 1. Methodological workflow of the study. The analysis proceeds in three phases. Phase 1 (data preparation) resamples all inputs to a common 0.05° grid, computes monthly SIF (solar-induced chlorophyll fluorescence) anomalies, detrends them, and selects stable forest pixels. Phase 2 (drought response assessment) identifies drought events from the 3-month Standardized Precipitation Evapotranspiration Index (SPEI-3), detects valid negative anomaly segments, and computes pixel-level resistance (Rt) and recovery (Rc) and their event-level trade-off. Phase 3 (modelling and interpretation) fits Random Forest models for Rt and Rc and a boosted regression tree (BRT) model for the trade-off, followed by variable-importance, SHAP (SHapley Additive exPlanations), and response-curve analysis. Input datasets are GOSIF v2 SIF, SPEI-3, forest integrity indicators (FLII and tree species diversity), and environmental predictors, all for 2001–2022.

3.2 Data sources and preprocessing

Monthly ecosystem productivity was represented by the GOSIF v2 monthly solar-induced chlorophyll fluorescence (SIF) dataset from January 2001 to December 2022 (Li & Xiao, 2019). SIF was selected because it is closely related to photosynthetic activity and reflects short-term changes in vegetation function during drought. Pixels were retained only when they had at least 264 valid monthly observations during the 22-year study period, ensuring a nearly complete time series for each pixel.

Drought conditions were represented by the 3-month Standardized Precipitation Evapotranspiration Index (SPEI-3). SPEI-3 was used because it captures short- to medium-term water deficits and is suitable for monthly drought-event detection (Vicente-Serrano et al., 2010). Drought events were identified independently for each pixel from the monthly SPEI-3 time series.

Annual forest cover from 2001 to 2016 was obtained from the MEaSUREs Vegetation Continuous Fields (VCF) product (Hansen & Song, 2018), which provides percent tree cover at 0.05° resolution. The annual tree-cover rasters were used only for the stable forest mask described in Section 3.3.

FLII was obtained as a published global product from Grantham et al. (2020) and was not computed in this study. It serves as the indicator of forest integrity at the landscape level, integrating observed human pressures, inferred indirect pressures, and loss of forest connectivity into a single score from 0 (most modified) to 10 (least modified) at ~300-m resolution. In this study, the original raster was resampled to the 0.05° master grid using average resampling.

Tree species diversity was used as the indicator of forest integrity at the species level. The data were obtained from the global tree species richness map of Liang et al. (2022), which estimates local species richness per hectare at 0.025° resolution from approximately 1.3 million sample plots and 55 million trees archived in the Global Forest Biodiversity Initiative database. The raster was aggregated to the 0.05° master grid using a 2 × 2 block-mean approach.

Climate predictors were derived from the ERA5-Land reanalysis (Muñoz-Sabater et al., 2021) for 2001–2022. For each variable, monthly values were aggregated to annual values, and the final predictor was calculated as the multi-year mean. The climate predictors included mean annual temperature (MAT), mean annual precipitation (MAP), the coefficient of variation of

annual precipitation (CV_MAP), mean vapour pressure deficit (VPD), and the aridity index (AI, calculated as the ratio of annual precipitation to annual potential evapotranspiration). All variables were resampled from the native ERA5-Land grid to the 0.05° master grid using bilinear interpolation implemented via xarray.DataArray.interp.

Three event-level predictors were calculated to describe the local drought and climate conditions associated with each pixel's effective drought events. Drought severity was defined as the negative sum of SPEI-3 values within each drought window, with larger values indicating more severe droughts. Temperature and precipitation anomalies were calculated as standardized anomalies (z-scores relative to the 2001–2022 same-calendar-month climatology) using ERA5-Land 2-m air temperature and total precipitation, then averaged within each drought window. For each pixel, the median across all effective events was used as the final predictor. These three variables served as control variables to account for differences in drought intensity and drought-window climate conditions across pixels; they did not affect the calculation of resistance, recovery, or the trade-off.

Topsoil sand fraction (%) was obtained from the Harmonized World Soil Database v1.2 (HWSD; FAO/IIASA/ISRIC/ISS-CAS/JRC, 2012), specifically the *T_SAND* variable representing the sand content of the topsoil layer (0–30 cm depth). The HWSD data were provided at a native resolution of 30 arc-seconds (~1 km). The *T_SAND* layer was resampled to the 0.05° master grid using bilinear interpolation, and values were constrained to the physically valid range of 0–100%. Elevation and slope were derived from the EarthEnv global topographic dataset (Amatulli et al., 2018) based on the GMTED2010 digital elevation model at 250 m resolution. Both were resampled to the 0.05° master grid using average resampling.

3.3 Stable forest mask

Stable forest pixels were identified from the annual percent tree cover time series for 2001–2016. The approach followed the time-series logic of Song et al. (2018), who used long-term annual fractional cover and Mann–Kendall trend tests to detect significant land-cover change. The purpose was to reduce the influence of deforestation, afforestation, and forest degradation on the calculation of drought resilience metrics.

The stable forest mask was constructed in two steps. First, a forest mask was defined: a pixel was classified as forest only when its tree cover was at least 20% in every year from 2001 to 2016. This strict all-year criterion excluded pixels that were forested only temporarily or that crossed the forest threshold during the observation period. Second, a Mann–Kendall trend test

was applied to each pixel's annual tree-cover series, and pixels with a significant trend ($p < 0.05$) were excluded. A pixel was considered a stable forest only if it had valid annual records, tree cover ≥ 20% in every year, and no significant trend in tree cover during 2001–2016. This definition is conservative because it requires continuous forest presence and excludes pixels with statistically significant changes in tree cover.

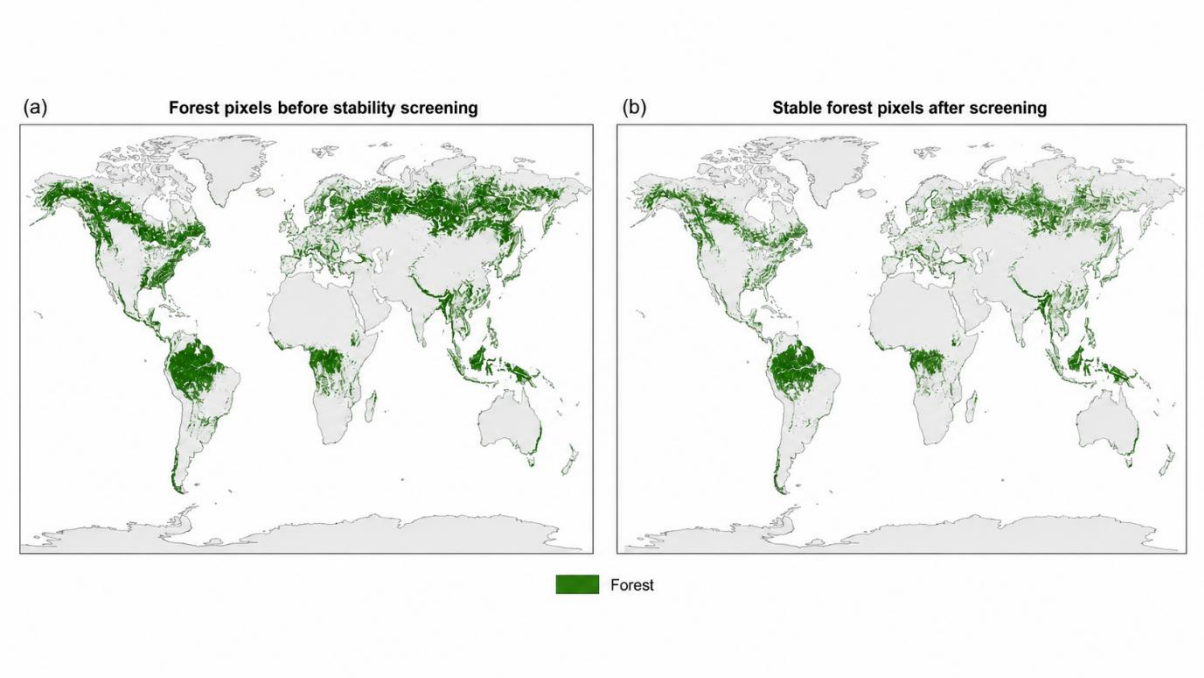

Figure 2. Forest pixels before and after stable forest screening. Global distribution of forest pixels at 0.05° resolution; green denotes forest. (a) All forest pixels from the MEaSUREs Vegetation Continuous Fields product (Hansen & Song, 2018), i.e. pixels with at least 20% tree cover. (b) Stable forest pixels retained after screening: tree cover ≥ 20% in every year from 2001 to 2016 and no significant trend in annual tree cover (Mann–Kendall test, $p \geq 0.05$). The screening removes pixels affected by deforestation, afforestation, or degradation so that drought-resilience metrics are computed only over forests that remained stable during the study period.

3.4 Drought resilience metrics

Drought resilience metrics were calculated at the pixel level using monthly SPEI-3 and detrended GOSIF anomaly time series. This section included three steps: drought event identification, calculation of resistance and recovery, and estimation of the resistance–recovery trade-off.

Drought events were identified independently for each pixel using the SPEI-3 time series from 2001 to 2022. A drought event was defined as a continuous period in which SPEI-3 was lower than −1 for at least two consecutive months. The first month of this period was defined as the drought onset (d_0), and the last month was defined as drought termination (d_1). Events

shorter than two months were excluded because they were unlikely to represent sustained water stress at the monthly scale.

SIF anomalies: For each pixel, the long-term monthly climatology was calculated for each calendar month during 2001–2022. The SIF anomaly was then computed as the difference between the monthly GOSIF value and its corresponding monthly climatology, thereby removing the regular seasonal cycle. A linear detrending step was applied to the anomaly series to reduce the residual influence of long-term vegetation changes. The detrended anomaly series was used in all subsequent calculations.

Valid vegetation response:For each drought event, a valid vegetation response was required before resistance and recovery were calculated. A response was considered valid only when a continuous negative SIF anomaly segment occurred during the response search window, and the minimum anomaly within this segment was ≤ −0.5 standard deviations of the pixel-level anomaly series. This threshold excluded weak fluctuations around zero and retained events with a clear negative vegetation response. When more than one valid segment occurred within the search window, the segment with the deepest minimum was selected.

The time of minimum ecosystem productivity, t_{min}, was searched from drought onset to at most three months after drought termination. This extension allowed for a delayed productivity decline after the end of the meteorological drought. If another drought event began within this extended window, the search window ended before the next event to avoid overlap.

The resistance period began at the onset of productivity decline. If the SIF anomaly at drought onset was already non-positive, the resistance period began at that time. If the SIF anomaly at drought onset was greater than zero, the resistance period began in the first month after drought onset, when the anomaly fell to zero or below. This adaptive rule avoided counting months before ecosystem productivity had started to decline.

The time from the start of the resistance period to $t_{min}$was defined as T_1. The normalized vegetation loss during the resistance period was calculated as:

$$NL_{T1} = \frac{\left|V_{min} - V_{T1,start}\right|}{\overline{V}} \quad (1)$$

where $V_{min}$is the minimum detrended SIF anomaly during the selected negative anomaly segment, $V_{T1,start}$is the anomaly value at the start of the resistance period, and $\bar{V}$ is the long-term mean GOSIF value of the pixel during 2001–2022. Resistance was then calculated as:

$$Rt = \frac{T_1}{NL_{T1}} \quad (2)$$

A higher resistance indicates that ecosystem productivity declined more slowly relative to the magnitude of normalized vegetation loss.

Recovery was calculated after t_{min}. The recovery endpoint was defined as the first month after $t_{min}$when the detrended SIF anomaly returned to zero or above. The recovery period was not allowed to cross into the next drought event. The time from t_{min} to the recovery endpoint was defined as T_2. The normalized vegetation loss for the recovery period was calculated as:

$$NL_{T2} = \frac{|V_{min}|}{\overline{V}} \quad (3)$$

Recovery was then calculated as:

$$Rc = \frac{NL_{T2}}{T_2} \quad (4)$$

A higher recovery indicates faster recovery per unit of normalized vegetation loss. For each pixel, event-level resistance and recovery values were summarized as their median values. Median values were used to reduce the influence of unusually extreme drought events.

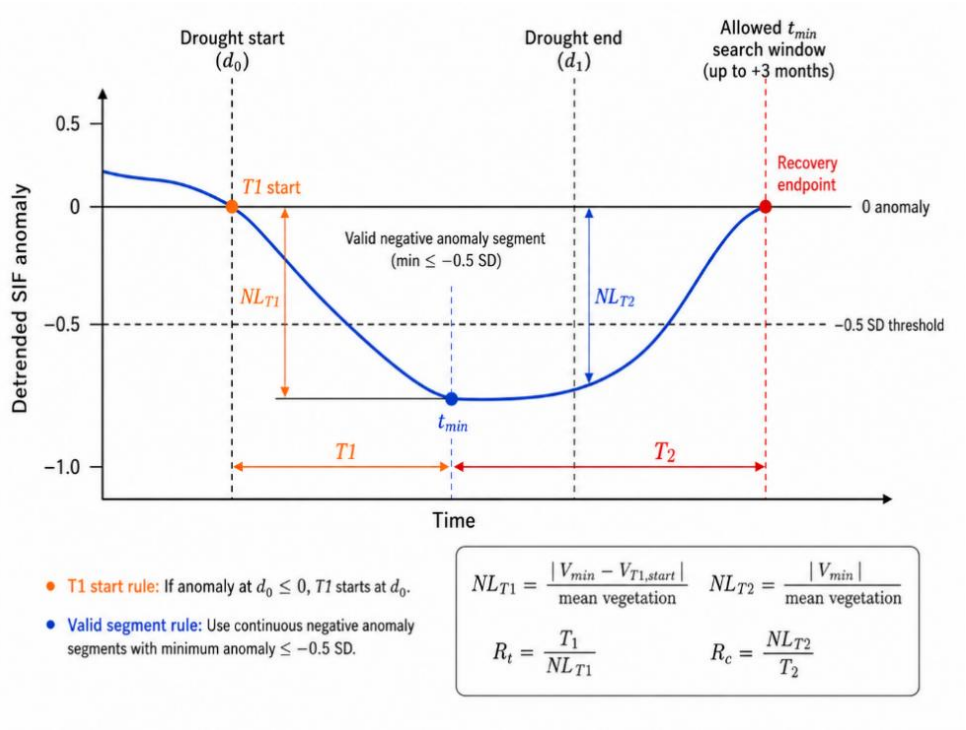

Figure 3. Conceptual diagram of resistance and recovery calculation. The diagram illustrates the start of the drought (d_0), drought termination (d_1), the allowed t_{min} search window up to three months after drought termination, the selected valid negative anomaly segment, and the definitions of T_1, T_2, NL_{T1}, and NL_{T2}. A segment was considered valid if the minimum detrended SIF anomaly was lower than or equal to −0.5 SD. Resistance and recovery were calculated as $\mathrm{Rt} = T_1/NL_{T1}$ and $Rc = NL_{T2}/T_2$, respectively.

The resistance–recovery trade-off was calculated using paired event-level R_t and R_c values within each pixel. Only pixels with at least five valid drought events were used for this calculation. This requirement reduced the risk of estimating correlations from too few event pairs while retaining sufficient global coverage. For each eligible pixel, both Pearson and Spearman correlations between event-level R_t and R_c were calculated. Pearson correlation was used as the main trade-off metric, while Spearman correlation was used as a rank-based consistency check.

A negative correlation indicates a trade-off between resistance and recovery. In this case, higher resistance tends to be associated with lower recovery, or lower resistance tends to be associated with faster recovery. For the trade-off model, only pixels with both Pearson < 0 and Spearman < 0 were retained. This restriction ensured that the trade-off analysis focused on pixels with a consistent negative relationship between resistance and recovery. The model target was defined as:

$$\text{trade-off strength} = -r_{Pearson}(Rt, Rc) \quad (5)$$

Thus, larger trade-off strength values represent stronger negative relationships between resistance and recovery.

3.5 Model table construction and predictor screening

Model tables were constructed based on the drought resilience metrics, and all predictor layers were aligned to a common 0.05° grid. The construction followed a common-sample logic to ensure that resistance, recovery, and trade-off analyses were based on comparable pixels.

A common base table was first built from stable forest pixels. A pixel was retained only when it had at least five valid drought-response events, positive and finite median resistance and recovery values, valid Pearson and Spearman correlations between event-level resistance and recovery, and finite values for all selected predictors. The Pearson and Spearman correlations were required to be finite and within the range [−1, 1], but were not required to be negative. This allowed the resistance and recovery models to represent all valid stable forest pixels, rather than only those with a negative resistance–recovery relationship.

The event-level drought and climate predictors were then merged into the base table by pixel coordinates. These included median drought severity, median standardized temperature anomaly, and median standardized precipitation anomaly during drought events. When these predictors were used, the finite event counts supporting each predictor had to match the effective event counts used for the response variables. This ensured that the event-level predictors were calculated from the same effective drought events used in the response analysis.

Separate model tables were then constructed for the resistance/recovery models and the trade-off model. The resistance/recovery table retained all pixels that satisfied the common base-table criteria and had complete predictor values. The trade-off table was built as a stricter subset of the same sample, retaining only pixels with both Pearson < 0 and Spearman < 0, so that the trade-off model focused only on pixels showing a consistent negative relationship. The model target for the trade-off table was defined as in Eq. 5, where larger values indicate a stronger trade-off. Spearman correlation was used only as a consistency filter, not as a model target.

The initial candidate predictor set contained 15 variables representing forest integrity, forest structure, climate background, climate variability, topography, soil texture, and event-level drought conditions. Predictor redundancy was assessed using pairwise Pearson correlation and variance inflation factors. After this screening, CV_MAT was removed because it showed strong redundancy with MAT. The final model used 14 predictors: FLII, tree species diversity,

elevation, slope, soil sand fraction, MAP, AI, MAT, CV_MAP, VPD, tree cover, drought severity, temperature anomaly during drought events, and precipitation anomaly during drought events (Table 1). FLII and tree species diversity were treated as the two core forest-integrity variables; the others served as control variables for climate background, climate variability, drought-event conditions, topography, soil texture, and baseline forest cover.

Table 1. Summary of predictor variables used in the machine learning models. FLII and tree species diversity are the two core forest integrity variables; all other predictors serve as control variables. All variables were resampled or aggregated to the common 0.05° grid before modelling.

Category	Variable	Description	Data source	Native res.	Model role
Forest integrity	FLII	Forest Landscape Integrity Index (0–10)	Grantham et al. (2020)	~300 m	Core
Forest integrity	Tree species diversity	Tree species richness per hectare	Liang et al. (2022)	0.025°	Core
Climate background	MAT	Mean annual temperature (°C)	ERA5-Land; Muñoz-Sabater et al. (2021)	0.1°	Control
Climate background	MAP	Mean annual precipitation (mm)	ERA5-Land	0.1°	Control
Climate background	CV_MAP	CV of annual precipitation	ERA5-Land	0.1°	Control
Climate background	VPD	Mean vapour pressure deficit (kPa)	ERA5-Land	0.1°	Control
Climate background	AI	Aridity index (MAP / PET)	ERA5-Land	0.1°	Control
Event-level drought	Drought severity	Median negative sum of SPEI-3 during drought events	Derived from SPEI-3	0.05°	Control
Event-level drought	Temperature anomaly	Median standardized temperature anomaly during drought events	Derived from ERA5-Land	0.05°	Control
Event-level drought	Precipitation anomaly	Median standardized precipitation anomaly during drought events	Derived from ERA5-Land	0.05°	Control
Topography	Elevation	Mean elevation (m)	EarthEnv; Amatulli et al. (2018)	250 m	Control
Topography	Slope	Mean slope (°)	EarthEnv; Amatulli et al. (2018)	250 m	Control
Soil	Soil sand fraction	Topsoil sand content (%)	HWSD v1.2; FAO et al. (2012)	30 arc-sec	Control
Forest structure	Tree cover	Mean tree cover 2001–2016 (%)	VCF; Hansen & Song (2018)	0.05°	Control

Note: *Native resolution refers to the original spatial resolution of each dataset before resampling to the 0.05° master grid. Event-level drought predictors were derived at 0.05° grid resolution from the listed source datasets.*

Before modelling, median resistance and recovery values were transformed to reduce the influence of extreme values and improve model stability. Raw median values were first log-

transformed, then winsorized using the 0.5th and 99.5th percentiles, and finally standardized using z-scores. The z-score statistics were calculated after applying the final model-table mask.

The final outputs from this step included a common resistance/recovery model table, a trade-off model table, and diagnostic files for missingness, row counts, correlation matrices, VIF values, and target transformations. These diagnostic outputs were used to confirm that the final tables were complete and internally consistent before machine-learning modelling.

3.6 Machine-learning modelling and evaluation

Machine-learning models were used to quantify relationships between forest integrity and drought resilience metrics, accounting for climate, topography, soil, forest structure, and event-level drought conditions. Three resilience variables were modelled: drought resistance, drought recovery, and the strength of the resistance–recovery trade-off.

Random Forest models for resistance and recovery

Random Forest regression was used for resistance and recovery. RF was selected because it can capture nonlinear relationships and interactions among predictors while providing stable predictive performance for large ecological datasets. The two response variables were the transformed median resistance and recovery values (log-transformed, winsorized, and z-score standardized; see Section 3.5). Both models used the 14-variable predictor set described in Table 1.

To reduce the influence of spatial clustering, model training and evaluation were based on 80,000 pixels selected using 5° × 5° spatially stratified sampling. This strategy retained broad global spatial coverage while limiting the dominance of densely represented forest regions. The same sample was used for model evaluation and for the final sample-fit models used in the subsequent interpretation.

Model performance was evaluated using 10-fold cross-validation. In each fold, the model was trained on 90% of the sampled pixels and validated on the remaining 10%. Performance was summarized using the mean training R^2, validation R^2, root mean square error, and mean absolute error across folds.

SHAP analysis: SHAP (SHapley Additive exPlanations) values were computed for each predictor and each pixel in the 80,000-pixel spatial sample using the TreeExplainer method in the SHAP library (Lundberg et al., 2020), which provides exact SHAP values for tree-based

models. For each pixel, the SHAP value of a given predictor quantifies its marginal contribution to the deviation of the model prediction from the global mean, averaged across all possible predictor coalitions.

Global feature importance was summarised as the mean absolute SHAP value (mean |SHAP|) of each predictor across all sampled pixels, providing a model-agnostic ranking of predictor influence on spatial variation in drought resistance and recovery.

SHAP dependence plots were constructed by plotting the SHAP value of each predictor against its raw value across all sampled pixels, revealing the direction and nonlinearity of each predictor's marginal effect. Each dependence plot was coloured by the predictor exhibiting the strongest interaction with the focal predictor, as identified automatically by the SHAP library.

To further examine how the effects of forest-integrity variables varied across environmental contexts, pairwise SHAP interaction values were computed using the TreeExplainer method in the SHAP library (Lundberg et al., 2020). For each sample, the SHAP interaction matrix decomposes the total SHAP value of each predictor into a main effect and a set of pairwise interaction terms:

$$SHAP_i = \Phi_{ii} + \sum_{j \neq i} \Phi_{ij} \quad (6)$$

where SHAP_i is the total SHAP value for predictor *i*, Φ_ii is the main effect of predictor *i*, and Φ_ij is the interaction effect between predictors *i* and *j*. A positive Φ_ij indicates that the combined contribution of predictors *i* and *j* exceeds the sum of their individual main effects, while a negative Φ_ij indicates the opposite. The interaction matrix is symmetric (Φ_ij = Φ_ji), so the pair-total interaction value was defined as 2Φ_ij.

Because computing interaction values for all 80,000 samples is expensive, a random subsample of 1,000 pixels was drawn from the spatially stratified sample for interaction analysis. Pairwise interaction importance was ranked by the mean absolute pair-total interaction value across all sampled pixels. SHAP interaction dependence plots were used to visualize how the interaction contribution of a focal variable changed along its own gradient, with points coloured by the interacting variable.

BRT model for the resistance–recovery trade-off

Boosted regression tree modelling was performed using the *gbm.step* function in the R package *dismo*. Trade-off strength was defined as the negative Pearson correlation between event-level resistance and recovery (Eq. 5), with larger values indicating a stronger trade-off. Only pixels with negative values for both Pearson and Spearman correlations were retained. The BRT model used the same 14-variable predictor set and was trained on the same 80,000 spatially stratified pixels. The final BRT parameters were tree complexity = 12, learning rate = 0.01, bag fraction = 0.65, and minimum observations per node = 10. Model performance was evaluated using the built-in 10-fold cross-validation in *gbm.step*, and the squared cross-validated correlation was reported as the validation R^2.

For model interpretation, variable importance and SHAP-based analyses were conducted on the final sample-fit models trained on the same 80,000 spatially stratified pixels. This ensured consistency between model evaluation and interpretation.

4. Results

4.1 Analytical samples used for model analysis

After applying the stable forest mask, drought-event screening, response-metric validity criteria, and predictor completeness filtering, 611,540 stable forest pixels were retained for the resistance and recovery models. These pixels had at least five valid drought-response events, positive and finite median resistance and recovery values, valid Pearson and Spearman correlations between event-level resistance and recovery, and complete values for the final predictor set.

The trade-off analysis used a stricter subset of the same common sample. A total of 446,313 pixels showed both negative Pearson and negative Spearman correlations between event-level resistance and recovery, accounting for 72.98% of the resistance/recovery modelling sample. This subset was used to model trade-off strength, defined as the negative Pearson correlation; larger values indicate a stronger negative relationship between resistance and recovery (Table 2).

This sample design allowed resistance and recovery to be modelled across all valid stable forest pixels, while the trade-off model focused only on pixels with a consistent negative relationship between the two drought resilience dimensions.

Table 2. Analytical samples used in the final models. The resistance and recovery models used all stable forest pixels with valid resistance, recovery, and trade-off information and complete predictor values (n = 611,540). The trade-off model used a stricter subset retaining only pixels with both Pearson and Spearman correlations between event-level resistance and recovery below zero (n = 446,313; 72.98% of the resistance/recovery sample). All pixels had at least five valid drought events.

Model target	Sample definition	Number of pixels
Resistance	Stable forest pixels with valid resistance, recovery, trade-off information, and complete predictors	611,540
Recovery	Stable forest pixels with valid resistance, recovery, trade-off information, and complete predictors	611,540
Trade-off strength	Subset with Pearson < 0 and Spearman < 0 between event-level resistance and recovery	446,313

4.2 Spatial patterns of forest drought resistance and recovery

Drought resistance and recovery showed clear, yet contrasting, spatial patterns across global stable forests (Figure 4).

Median resistance was relatively high in many tropical and subtropical forests, with higher values found mainly in the Amazon Basin, central Africa, and Southeast Asia. In contrast, lower resistance was widespread across high-latitude forests, especially in northern North America and northern Eurasia. These patterns suggest that tropical forests maintained ecosystem productivity more effectively during drought, while boreal forests showed weaker resistance.

The spatial pattern of recovery was different. Median recovery was relatively high in many boreal and temperate forests, particularly in northern North America and northern Eurasia, and in some dry or seasonally water-limited areas, including parts of western North America and southern Africa. Lower recovery values were common in humid tropical forests, including the Amazon Basin, central Africa, and Southeast Asia.

Overall, resistance and recovery showed a broad spatial contrast. Tropical forests tended to have higher resistance but lower recovery, whereas boreal and temperate forests often showed the opposite pattern. This indicates that forests with a stronger capacity to maintain function during drought did not necessarily recover faster afterwards, motivating the trade-off analysis in the next section.

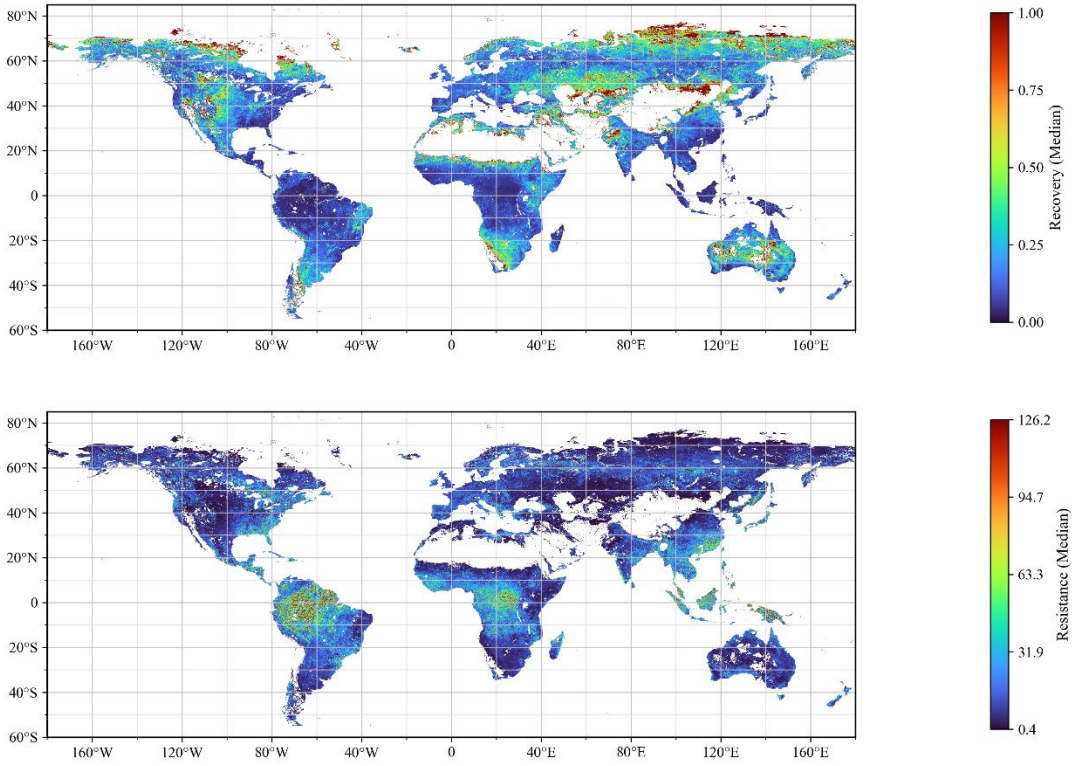

Figure 4. Global spatial patterns of median forest drought recovery and resistance. Results are shown for 611,540 stable forest pixels at 0.05° resolution over 2001–2022. (a) Median recovery (Rc) and (b) median resistance (Rt), both dimensionless and shown as the per-pixel median across all valid drought events (each pixel having at least five events). Resistance and recovery were derived from detrended GOSIF v2 solar-induced chlorophyll fluorescence anomalies and SPEI-3-based drought events. Warmer colours indicate higher values; note that the two panels use different colour scales (recovery 0–1; resistance 0.4–126.2).

4.3 Spatial pattern of the resistance–recovery trade-off

The trade-off between resistance and recovery was assessed by calculating the Pearson correlation between event-level resistance and recovery at each pixel (Figure 5). Negative correlations were widespread across global stable forests, indicating that higher resistance during a drought event was often associated with slower recovery afterwards.

Although the strength of the correlation varied spatially, the overall pattern suggests that the resistance–recovery trade-off was a widespread feature of global stable forests rather than a regional phenomenon. Based on the screening criteria described in Section 3.4, 446,313 pixels were retained for the trade-off analysis, accounting for 72.98% of the full resistance/recovery modelling sample. For these pixels, trade-off strength was defined as the negative Pearson correlation, so that larger values represent a stronger negative relationship between resistance and recovery.

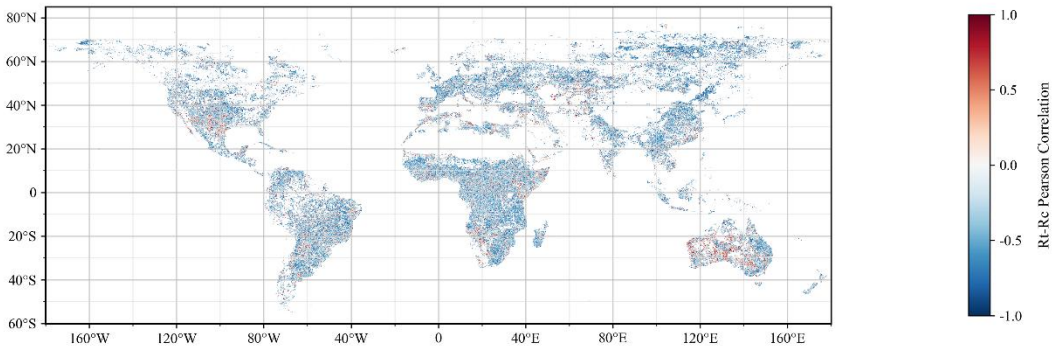

Figure 5. Global spatial pattern of the pixel-level Pearson correlation between event-level forest drought resistance and recovery. The correlation between event-level resistance (Rt) and recovery (Rc) is shown for stable forest pixels with at least five valid drought events (0.05° resolution, 2001–2022). Blue indicates a negative correlation (a resistance–recovery trade-off, i.e. higher resistance associated with slower recovery within a pixel); red indicates a positive correlation. Negative correlations dominate across global stable forests.

4.4 Model performance

The machine-learning models showed varying predictive performance for resistance, recovery, and trade-off strength (Table 3). Random Forest models were used for resistance and recovery, and a BRT model for the trade-off.

The Random Forest model for recovery showed the highest predictive performance among the three response variables, with a mean training R^2 of 0.850 and a mean validation R^2 of 0.625 across the 10-fold cross-validation. This suggests that the model captured substantial spatial variation in recovery while maintaining acceptable validation performance.

The resistance model also showed moderate predictive performance, with a mean training R^2 of 0.773 and a mean validation R^2 of 0.555. The mean train–validation gap was 0.218, close to that of the recovery model. These results indicate that the selected predictors explained a meaningful proportion of the spatial variation in both drought resilience dimensions, with slightly stronger performance for recovery than for resistance.

The BRT model for trade-off strength showed lower predictive performance than the resistance and recovery models. The training R^2 was 0.083, and the cross-validated correlation was 0.206, giving a squared cross-validated correlation of 0.043. This indicates that trade-off strength was more difficult to predict from the selected predictors and that its temporal relationship may be influenced by event-level or local processes not fully captured by the current predictor set.

Overall, model performance was stronger for the two direct drought resilience metrics than for trade-off strength. The following sections therefore focus mainly on the predictor importance

and SHAP patterns for resistance and recovery, with the trade-off model treated as a complementary result.

Table 3. Model performance for drought resistance, recovery, and trade-off strength. Random Forest (RF) models were used for resistance (Rt) and recovery (Rc); a boosted regression tree (BRT) model was used for trade-off strength. Values are means across 10-fold cross-validation on the 80,000-pixel spatially stratified sample. Training R^2 and validation R^2 indicate the proportion of variance explained on the training and held-out folds, respectively; RMSE, root mean square error; MAE, mean absolute error. For the BRT model, validation R^2 is the squared cross-validated correlation.

Response variable	Model	Model sample size	Training R^2	Validation R^2	RMSE	MAE
Resistance (Rt)	Random Forest	80,000	0.773	0.555	0.673	0.530
Recovery (Rc)	Random Forest	80,000	0.850	0.625	0.635	0.495
Trade-off strength	BRT	80,000	0.083	0.043	0.205	0.167

4.5 Predictor importance for forest drought resistance and recovery

The SHAP analysis showed that resistance and recovery were influenced by different combinations of climate background, forest structure, and forest-integrity variables (Figure 6).

For resistance, mean annual precipitation was the most important predictor, followed by mean annual temperature and tree cover. Tree species diversity ranked fourth, while FLII contributed less. This pattern indicates that the ability of forests to maintain photosynthetic activity during drought was mainly associated with long-term hydroclimatic conditions and forest structural state. The high ranking of tree species diversity suggests that species-level forest integrity also contributed to spatial variation in resistance after climate, topography, soil, and drought-event conditions were considered.

For recovery, mean annual temperature was the strongest predictor, followed by tree cover, mean annual precipitation, and tree species diversity. Compared with resistance, recovery showed a stronger dependence on temperature and tree cover, suggesting that post-drought recovery was more closely related to thermal background and canopy structure than to precipitation alone.

Forest-related variables made clear contributions to both models. Tree cover ranked among the top predictors for both resistance and recovery, indicating that baseline forest structure was closely associated with drought resilience. Tree species diversity also ranked highly in both

models, suggesting a consistent association between species-level integrity and the two dimensions of drought resilience. FLII showed lower mean SHAP importance than tree species diversity in both models. Event-level drought variables — drought severity, precipitation anomaly, and temperature anomaly — showed relatively low mean SHAP importance in both models.

Overall, these results indicate that resistance and recovery were shaped by both environmental constraints and forest condition. Resistance was mainly associated with precipitation, temperature, and tree cover, while recovery was mainly associated with temperature, tree cover, and precipitation. Tree species diversity was consistently important for both resilience metrics, and FLII showed a weaker direct contribution. The direction and shape of these predictor effects are examined in the following sections.

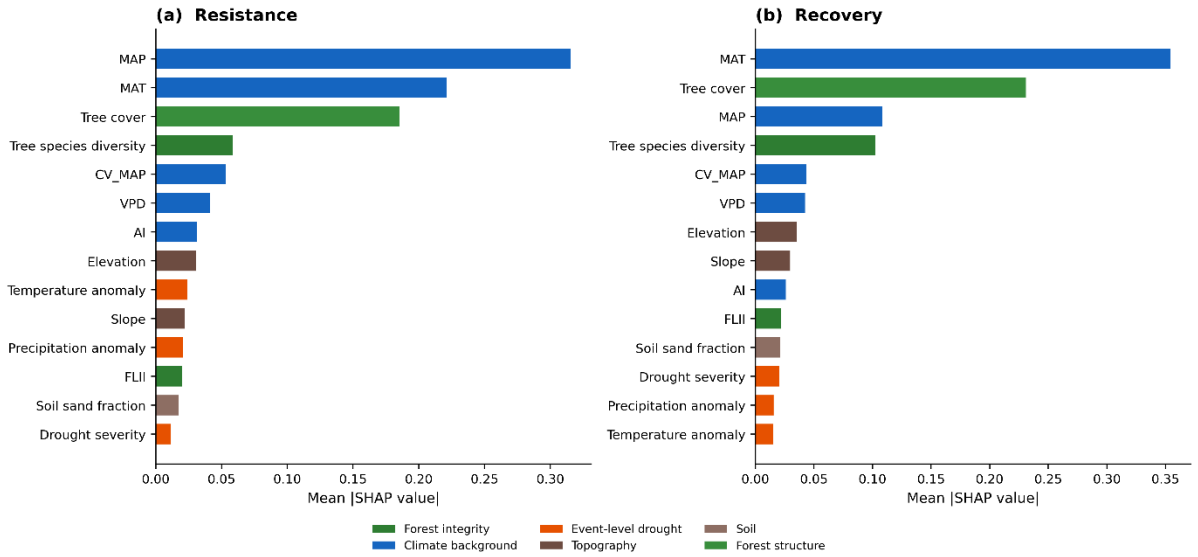

Figure 6. SHAP-based predictor importance for forest drought resistance and recovery. Bars show the mean absolute SHAP (SHapley Additive exPlanations) value of each of the 14 predictors in the Random Forest models of (a) resistance and (b) recovery, ordered from most to least important, based on the 80,000-pixel spatially stratified sample. A larger mean absolute SHAP value indicates a stronger average contribution to spatial variation in the predicted metric. Bar colours denote predictor categories (forest integrity, climate background, event-level drought, topography, soil, and forest structure), as shown in the legend.

4.6 SHAP responses of forest integrity variables

The SHAP dependence plots showed clear differences between the two forest-integrity variables (Figure 7).

FLII showed weak but distinguishable effects on resistance and recovery. Regarding resistance, the smoothed SHAP curve remained mostly negative across the FLII gradient, indicating a

generally negative marginal contribution (Figure 7a). The curve showed a gradual upward trend from low to high FLII values, approaching zero only at the highest end of the FLII range. This suggests that forests with lower landscape integrity tended to have slightly lower predicted resistance, while higher FLII values partially offset this negative contribution. For recovery, the FLII response was largely flat and centred around zero across the full range, with no clear directional trend (Figure 7c). These patterns are consistent with the lower mean SHAP importance of FLII shown in Figure 6.

Tree species diversity showed a stronger, more nonlinear relationship with both drought resilience metrics. In terms of resistance, low-diversity forests generally had negative SHAP values, especially when tree species diversity was below approximately 30–40 species (Figure 7b). The smoothed response curve increased after this range and became mostly positive at higher diversity levels, indicating that higher tree species diversity was associated with higher predicted resistance.

The response of recovery to tree species diversity showed an opposite pattern. At very low diversity values, the SHAP values were positive, but the smoothed curve declined as diversity increased (Figure 7d). At intermediate and high levels of diversity, tree species diversity showed increasingly negative SHAP values for recovery. This indicates that higher tree species diversity was associated with lower predicted recovery. The effect of diversity was therefore not uniformly positive across the two dimensions of drought resilience.

The opposite responses of resistance and recovery to tree species diversity also align with the spatial patterns shown earlier in this chapter. Tropical and subtropical forests generally showed higher resistance but lower recovery, whereas boreal and temperate forests often showed the opposite pattern. Because tree species diversity is also higher in many tropical forests, part of the negative relationship between diversity and recovery may reflect the broader biogeographic context in which high-diversity forests occur.

Overall, the two forest-integrity variables played different roles in the models. Tree species diversity showed a clearer species-level signal, with positive effects on resistance and negative effects on recovery. FLII showed weaker direct effects.

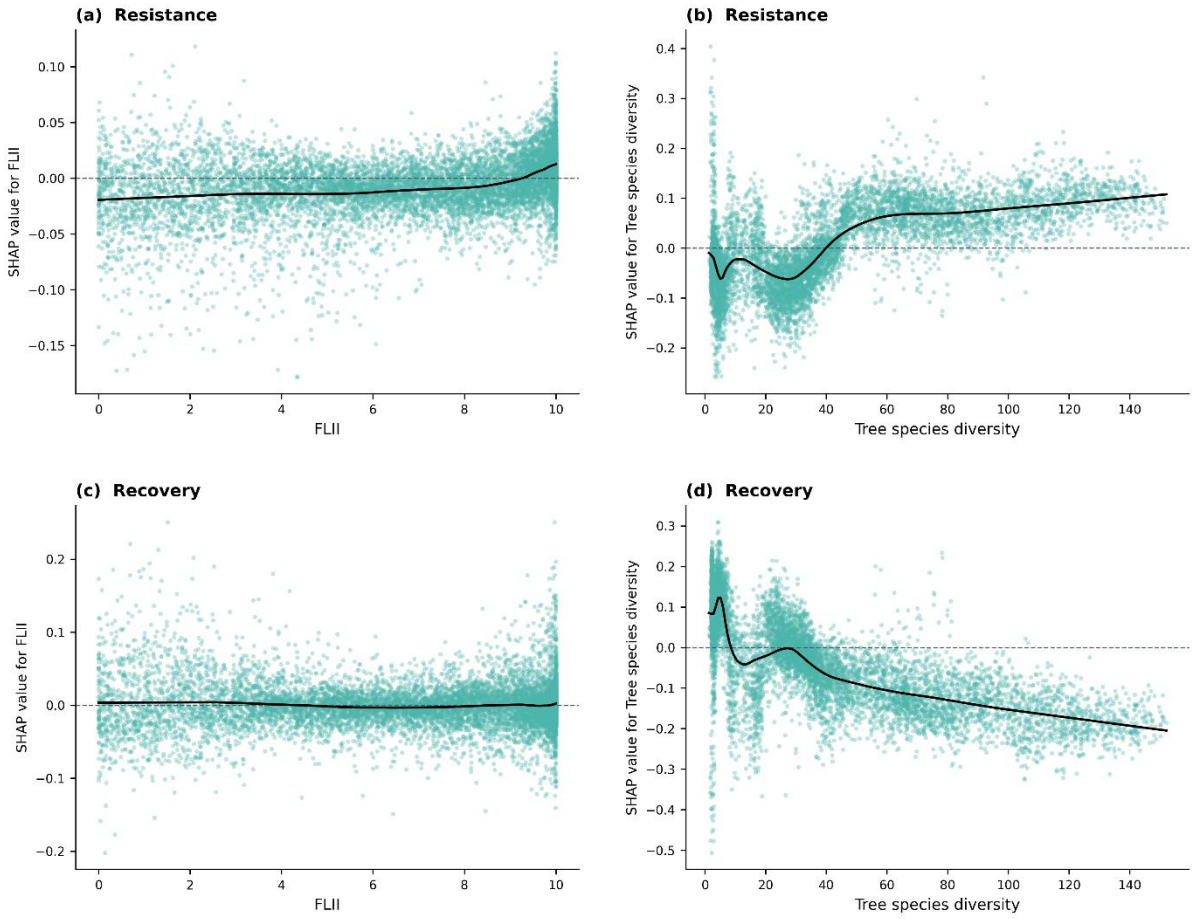

Figure 7. SHAP dependence plots for forest-integrity predictors in forest drought resistance and recovery models. Each panel shows the **main effect** SHAP value of a predictor (y-axis) against its raw value (x-axis) for every pixel in the 80,000-pixel spatially stratified sample (coloured points); the black line is a smoothed trend. Panels show FLII (Forest Landscape Integrity Index) for (a) resistance and (c) recovery, and tree species diversity (species per hectare) for (b) resistance and (d) recovery. Positive SHAP values indicate that a given predictor value raised the predicted metric above the sample mean, negative values that it lowered it.

4.7 Environmental control of forest drought resistance and recovery

The dependence plots of the dominant non-integrity predictors showed that resistance and recovery were also strongly conditioned by climate background and forest structure (Figure 8). This is consistent with the SHAP importance analysis, which found that MAP, MAT, and tree cover ranked among the most important predictors for both resilience metrics.

Regarding resistance, MAP showed a strong, positive, and nonlinear relationship with predicted resistance (Figure 8a). Forests in drier regions (MAP below approximately 1,000 mm) had strongly negative SHAP values, while the contribution increased steeply with precipitation and levelled off at higher MAP values. MAT showed a similar positive pattern, with cold forests

having negative SHAP values and warm forests having positive values (Figure 8b). Tree cover showed a weaker but still visible positive contribution, with higher tree cover generally associated with slightly higher predicted resistance (Figure 8c). These patterns suggest that the ability of forests to maintain photosynthetic activity during drought depends not only on forest integrity but also on the hydrothermal environment and baseline canopy structure.

For recovery, the dominant predictors showed directions opposite those for resistance. MAT had a strong negative relationship with recovery: cold forests had positive SHAP values, while warm forests had negative values (Figure 8d). Tree cover also showed a negative pattern, with higher tree cover associated with lower predicted recovery (Figure 8e). Recovery showed a weaker and less directional response to MAP, with a small positive contribution at intermediate precipitation levels and slightly negative values at higher MAP (Figure 8f). These patterns indicate that post-drought recovery was shaped by ecological conditions distinct from those of resistance. Forests that maintained function well during drought did not necessarily recover rapidly afterwards.

Overall, the climate background and forest structure provide the broad conditions under which forest integrity operates. The next section examines whether the effects of forest integrity vary with these dominant environmental gradients.

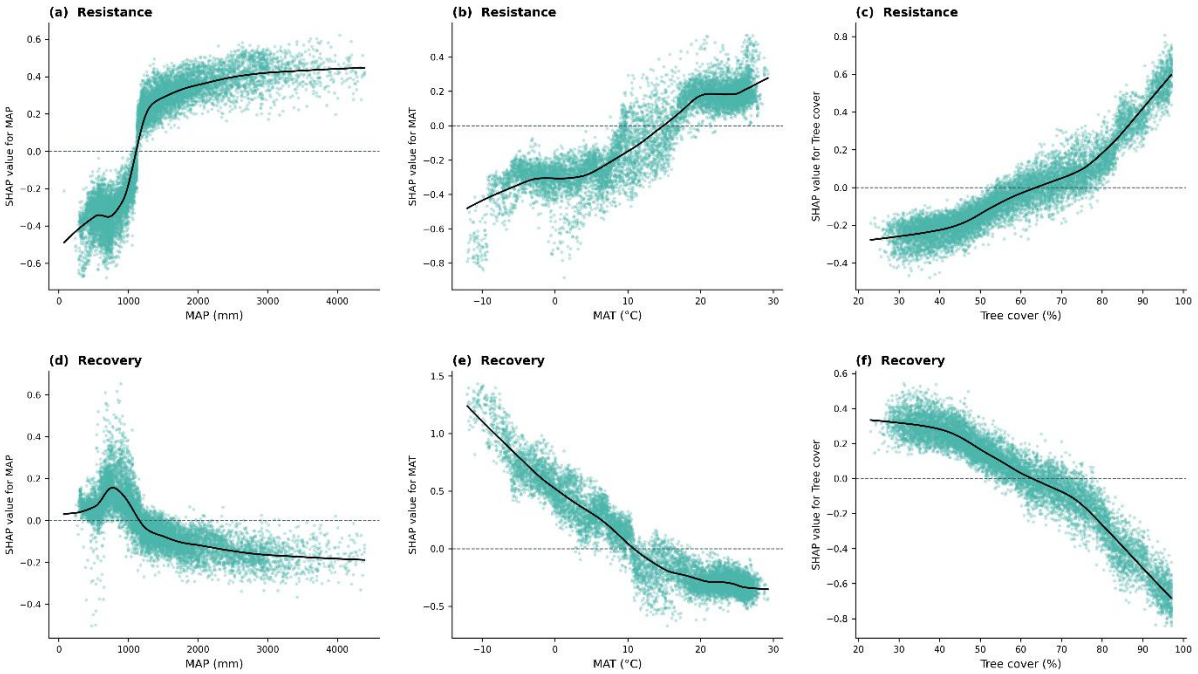

Figure 8. SHAP dependence plots for dominant environmental controls in forest drought resistance and recovery models. Each panel shows the total SHAP value of a predictor (*y*-axis) as a function of its raw predictor value (*x*-axis) across all sampled pixels. Panels (a)–(c) show results for the resistance model and panels (d)–(f) for the recovery model; columns correspond to MAP, MAT, and tree cover, respectively, for both rows.

4.8 Interactive effects between forest integrity and environmental context

In addition to the main SHAP effects, the interaction analysis showed that the effects of forest integrity were not independent of climatic and structural forest conditions (Figure 9). For resistance, the strongest interaction was between MAP and MAT, followed by MAP × tree cover, tree species diversity × MAP, and tree species diversity × MAT (Figure 9a). For recovery, the tree species diversity × MAT interaction had the highest interaction strength, followed by MAP × MAT and MAT × tree cover (Figure 9b). These results indicate that climatic gradients, especially temperature and precipitation, strongly modified the modelled effects of forest structure and species-level integrity on drought resilience. The interaction ranking differed between the two resilience metrics: resistance was more strongly shaped by climate–climate and climate–structure interactions, while recovery was more strongly shaped by the interaction between species diversity and temperature.

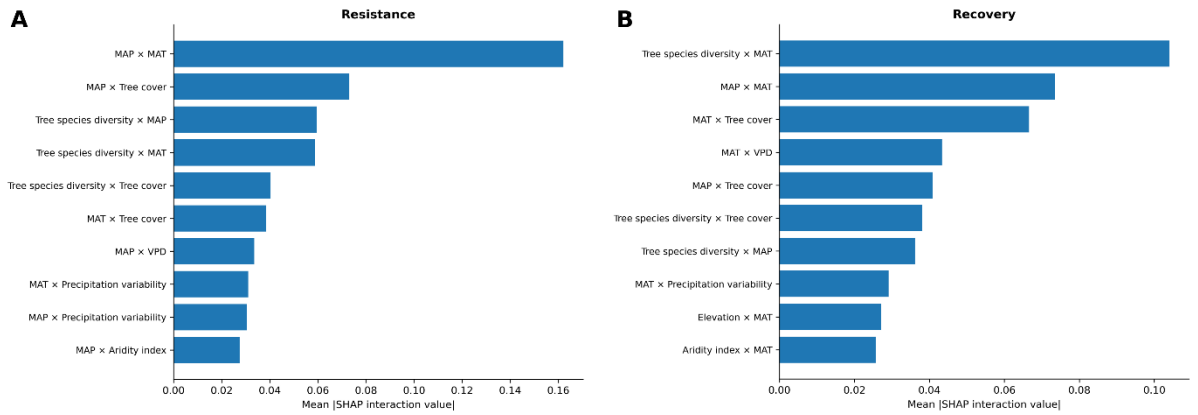

Figure 9. Top pairwise SHAP interaction strengths for forest drought (a) resistance and (b) recovery models, ranked by mean absolute pair-total interaction values. Bars show the mean absolute pair-total SHAP interaction value for each predictor pair, ranked from strongest to weakest, computed on a random subsample of 1,000 pixels drawn from the 80,000-pixel spatially stratified sample. A larger value indicates that the combined effect of the two predictors departs more strongly from the sum of their individual main effects. MAT, mean annual temperature; MAP, mean annual precipitation; VPD, vapour pressure deficit.

To examine how the effect of tree species diversity changed along environmental gradients, the SHAP interaction values for tree species diversity were plotted against three key environmental variables: MAT, MAP, and tree cover (Figure 10).

For resistance, the interaction between tree species diversity and MAT was generally negative across most of the diversity gradient, especially after tree species diversity exceeded approximately 40–50 species (Figure 10a). Since the main SHAP effect of tree species diversity on resistance was positive (Section 4.6), this negative interaction suggests that the positive contribution of diversity was reduced under warmer conditions — that is, the increase in predicted resistance associated with higher diversity was weaker in warm forests than in cool forests. The interaction with MAP showed a different pattern: the interaction value declined at low diversity levels, then increased and became mostly positive at intermediate and high diversity levels (Figure 10b). This suggests that precipitation may strengthen the positive effect of tree species diversity on resistance, especially when species richness is not extremely low. The interaction with tree cover showed positive values at low to moderate diversity levels but became weaker or negative at higher diversity levels (Figure 10c).

For recovery, these interactions showed contrasting directions. The interaction between tree species diversity and MAT was mostly positive, increasing rapidly at low to moderate diversity levels and remaining positive across most of the remaining gradient (Figure 10d). Since the main SHAP effect of diversity on recovery was negative (Section 4.6), this positive interaction suggests that warmer conditions partially offset the negative effect — the reduction in predicted

recovery associated with higher diversity was weaker under warmer conditions than under cooler conditions. The interaction with MAP was weaker and remained close to zero across most of the gradient (Figure 10e), indicating that precipitation had a less consistent modifying effect on the diversity–recovery relationship. The interaction between tree cover and species diversity was negative at low diversity levels and shifted toward positive values when tree species diversity exceeded approximately 50–60 species (Figure 10f), suggesting that high tree cover and high species diversity together may contribute more clearly to post-drought recovery than to resistance.

These interaction effects represent marginal modifications to the main SHAP contributions, not reversals of the overall spatial patterns described in Sections 4.2 and 4.7. Overall, species-level forest integrity affected resistance and recovery through different environmental contexts: the positive effect of diversity on resistance was weakened under warmer conditions, while its negative effect on recovery was partially offset under warmer conditions and modulated by tree cover.

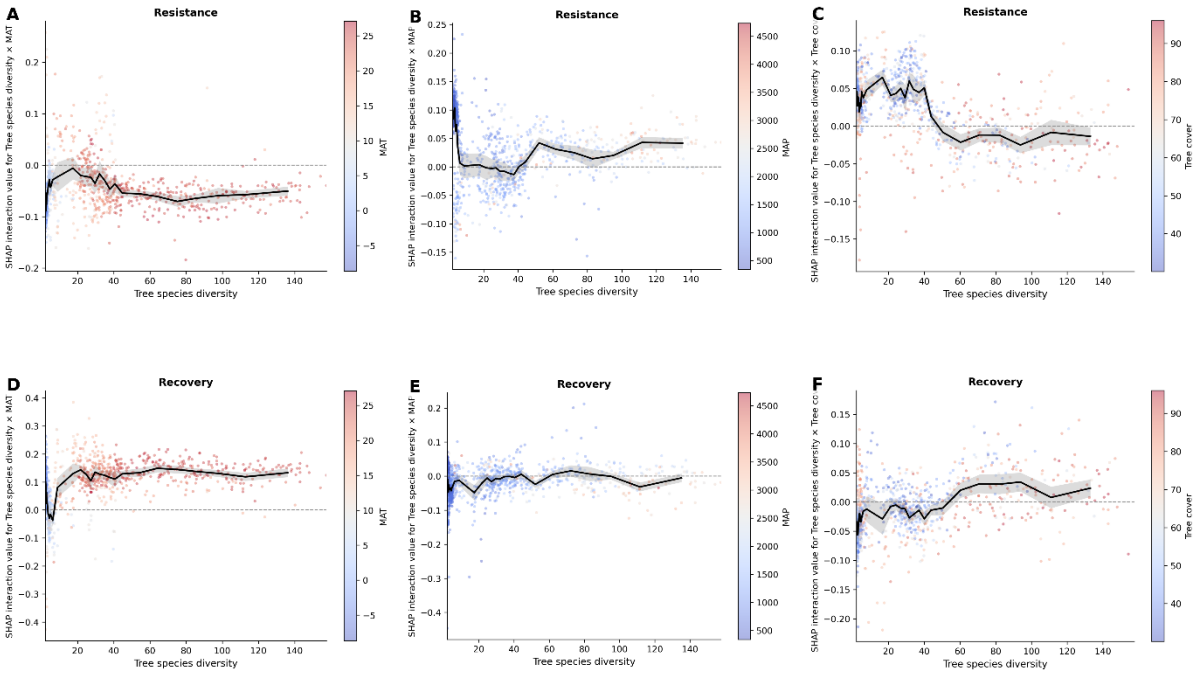

Figure 10. SHAP interaction dependence plots showing how the effect of tree species diversity changes along key environmental gradients. Each panel shows the pairwise SHAP interaction value between tree species diversity and a focal environmental predictor (x-axis) for individual pixels (coloured points), with point colour indicating the value of the focal environmental predictor as shown in the right-hand colour bar. The black line is a LOESS smoother (span = 0.28) summarising the overall trend, and the grey shaded band represents its 95% pointwise confidence interval. Panels (a)–(c) show results for the resistance model and panels (d)–(f) for the recovery model, with columns corresponding to MAP, MAT, and tree cover, respectively.

5. Discussion

5.1 Main findings

This study examined how forest integrity is associated with ecosystem resistance and recovery to drought across global stable forests. The results can be summarized in five main findings. First, resistance and recovery showed contrasting spatial patterns: tropical and subtropical forests generally had higher resistance but lower recovery, whereas boreal and temperate forests showed the opposite pattern. Second, the resistance–recovery trade-off was widespread, with negative temporal correlations observed in 72.98% of the modelling sample. Third, tree species diversity was a consistently important predictor of both resistance and recovery, but its effects were not uniformly positive — higher diversity was associated with higher resistance but lower recovery. Fourth, FLII showed a weaker direct contribution in both models, suggesting that landscape-level integrity may operate through distinct and more context-dependent pathways than species-level diversity. Fifth, the SHAP interaction analysis showed

that the effects of tree species diversity on drought resilience were modified by environmental gradients, especially temperature.

These findings provide only partial support for the original hypotheses. H1 (higher FLII → higher resistance and faster recovery) was weakly supported for resistance and not supported for recovery: FLII contributed only marginally to either model, and its dependence plot for recovery was essentially flat. H2 (higher tree species diversity → higher resistance and faster recovery) was supported for resistance but not for recovery: tree species diversity had a strong positive effect on resistance and a clear negative effect on recovery. The hypothesis that both dimensions of forest integrity would have parallel positive effects on the two components of resilience was therefore only partially confirmed. The unexpected negative association between species diversity and recovery, together with the limited direct contribution of FLII, motivates the more detailed interpretation in the following sections.

5.2 Resistance and recovery represent different dimensions of forest drought resilience

The contrasting spatial patterns of resistance and recovery suggest that these two metrics reflect different ecological processes. Resistance describes the ability of forests to maintain ecosystem productivity during drought. In this study, high resistance was more common in tropical and subtropical forests, which generally have high productivity, high canopy cover, and long growing seasons. Such conditions may allow forests to maintain photosynthetic activity during moderate drought events, especially where deep rooting systems, hydraulic redistribution, or species complementarity help stabilize ecosystem function.

However, high resistance did not necessarily imply high recovery. Recovery was generally lower in many humid tropical forests and higher in boreal and temperate forests. This pattern suggests that forests with strong drought resistance may experience smaller immediate declines, but their post-drought recovery can still be slow. One possible explanation is that in high-biomass and high-canopy systems, ecosystem productivity is already close to a high baseline state before drought (Hubau et al., 2020; Forzieri et al., 2022). After drought disturbance, recovery may be constrained by slow structural adjustment, lagged physiological stress, or delayed canopy-level responses. In contrast, forests in cooler regions may show stronger declines during drought but recover more rapidly once water limitation is relieved.

This finding is consistent with the idea that resistance and recovery are complementary but not interchangeable components of resilience (Hodgson et al., 2015; Ingrisch & Bahn, 2018). Resistance is more closely related to the capacity to buffer drought impacts during the event, while recovery is more closely related to the ability to regain function afterwards. These processes may depend on different mechanisms. Resistance may be supported by drought-tolerant traits, access to deeper soil water, high canopy stability, or functional complementarity (Anderegg et al., 2018). Recovery may depend more on growth rate, post-drought carbon balance, hydraulic repair, phenological flexibility, and the availability of favourable conditions after drought (Schwalm et al., 2017).

The widespread negative relationship between event-level resistance and recovery further supports this interpretation. In a large proportion of stable forest pixels, higher resistance was associated with lower recovery. This does not necessarily mean that resistance directly suppresses recovery. Instead, it may reflect the fact that the two metrics describe different phases of the drought response. Forests that lose little function during drought have less short-term recovery potential afterwards, while forests that experience a stronger decline can show larger apparent recovery if environmental conditions improve. The resistance–recovery trade-off should therefore be interpreted as a pattern in ecosystem response dynamics rather than a simple causal relationship.

The BRT model for trade-off strength showed much lower predictive performance than the models for resistance and recovery (validation $R^2 = 0.043$). This suggests that the spatial variation in trade-off strength was not well captured by the long-term environmental and forest-condition predictors used here. One possible explanation is that the temporal correlation between event-level resistance and recovery within each pixel depends on local, event-specific factors — such as the sequence and timing of drought events, antecedent soil moisture conditions, or species-specific physiological responses — that are not represented by the pixel-level median predictors (Schwalm et al., 2017; Xu et al., 2019). While the resistance–recovery trade-off is spatially widespread, its strength may therefore be driven by processes operating at finer temporal or ecological scales than the current modelling framework can resolve.

5.3 Species-level forest integrity has opposite effects on resistance and recovery

A central finding of this study is that tree species diversity was associated with higher resistance but lower recovery. This pattern was evident in both the SHAP importance ranking, where tree

species diversity ranked fourth for both resilience metrics, and the SHAP dependence plots, where the effect direction clearly differed between the two metrics (Figure 6).

The positive effect of tree species diversity on resistance is consistent with a growing body of evidence linking biodiversity to ecosystem stability under environmental stress (Isbell et al., 2015; Liu et al., 2022; Bai & Tang, 2024). Several mechanisms may explain this relationship. First, species-rich forests are more likely to contain species with complementary resource-use strategies, such as differences in rooting depth, water-use efficiency, or phenological timing. This niche complementarity can allow diverse communities to maintain aggregate photosynthetic activity even when some species are negatively affected by drought, although its magnitude varies with climate context (Grossiord et al., 2014). Second, hydraulic diversity — the range of drought-response strategies present in a community — has been shown to buffer ecosystem-level responses to water stress (Anderegg et al., 2018). In a diverse forest, drought-sensitive species may lose function while drought-tolerant species continue to photosynthesize, leading to a smaller overall decline at the ecosystem level. Third, species-rich communities may benefit from an insurance effect, where the probability that at least some species can maintain function under any given drought condition increases with the number of species present.

The negative effect of tree species diversity on recovery is less commonly reported in the literature, but it is not ecologically unexpected. Several non-exclusive explanations may account for this pattern. First, forests with higher species diversity tend to be located in tropical and subtropical regions, where ecosystem productivity is already close to a high baseline before drought (Liang et al., 2022; Hubau et al., 2020). When the pre-drought baseline is high, the absolute magnitude of post-drought recovery is constrained — there is simply less room for the signal of recovery to appear in the SIF-based metric. Second, diverse tropical forests tend to have high standing biomass and complex canopy structure. Recovery in such systems may require not only physiological recovery of individual trees but also structural readjustment of the canopy, which can be slow. Third, species-rich communities may include a wider range of recovery strategies: some species may recover quickly, while others recover slowly or not at all within the observation window. The aggregate recovery signal may therefore appear weaker than in less diverse forests dominated by fast-recovering species. Fourth, the same traits that promote resistance — such as conservative water use, high wood density, and deep rooting — are often associated with slower growth rates. Species that resist drought effectively may simply take longer to return to pre-drought activity levels, resulting in lower measured recovery.

These opposing effects may represent two sides of the same ecological mechanism. Forests that maintain function during drought — because of complementary resource use or hydraulic diversity — experience smaller initial declines. But smaller declines leave less room for detectable recovery, and the same conservative strategies that support resistance may slow post-drought regrowth. This interpretation is consistent with the resistance–recovery trade-off observed at the pixel level (Section 4.3) and with the broader idea that different components of ecosystem stability may be governed by partially conflicting ecological processes (Hillebrand et al., 2018).

It is important to note that the negative association between tree species diversity and recovery does not necessarily mean that diversity hinders recovery in a causal sense. Because tree species diversity is strongly correlated with tropical location, the negative recovery signal may partly reflect the climatic and structural conditions of tropical forests rather than a direct effect of species diversity itself. The SHAP analysis accounts for other variables in the model, but it cannot fully eliminate confounding between diversity and the broader environmental context. Therefore, the diversity–recovery relationship should be interpreted as a conditional association within the modelling framework, not as evidence that reducing diversity would improve recovery.

5.4 Landscape-level forest integrity and the role of FLII

FLII showed a weaker direct contribution to resistance and recovery than tree species diversity, ranking tenth and thirteenth in the SHAP importance analysis, respectively. The SHAP dependence plots confirmed that the marginal effect of FLII was small across most of its range, with only a slight positive shift in resistance at the highest FLII values. This result may seem surprising given that landscape-level forest integrity is widely considered important for ecosystem functioning (Grantham et al., 2020; Watson et al., 2018). However, several methodological and ecological factors may explain this pattern.

First, FLII and tree cover are correlated. Forests with high canopy cover tend to be located in landscapes with less fragmentation and lower human pressure, which are the same conditions captured by high FLII values. In the Random Forest models, tree cover consistently ranked among the top three predictors for both resistance and recovery. When a strongly predictive variable that shares variance with FLII is already in the model, the additional explanatory power of FLII is reduced. SHAP distributes the shared contribution between correlated predictors, and the variable with the stronger marginal signal — in this case, tree cover —

captures most of the shared variance. This means that the low SHAP importance of FLII does not necessarily reflect a weak ecological role, but rather that its signal overlaps with tree cover within the current modelling framework.

Second, there may be a scale mismatch between FLII and the resilience metrics. FLII is a landscape-level index that integrates information on forest connectivity, edge effects, and human modification across broader spatial extents (Grantham et al., 2020). The resilience metrics in this study — pixel-level median resistance and recovery — were measured at 0.05° resolution. The effects of landscape integrity on ecosystem function may operate at spatial scales smaller than individual pixels, for example, through cross-boundary hydrological processes, microclimate buffering by surrounding forest cover (De Frenne et al., 2019), or edge-mediated stress exposure (Banbury, Morgan & Jucker, 2025; Koelemeijer et al., 2023). These finer-scale mechanisms may not be fully captured by a pixel-level modelling framework.

Third, the effect of FLII may be more context-dependent than that of tree species diversity. The SHAP dependence plots showed that FLII had a near-zero effect across most of its range, with a positive contribution appearing only at very high values. This suggests that landscape integrity may function less as a continuous gradient and more as a threshold condition: forests in highly intact landscapes may gain some additional resilience, but moderate differences in FLII do not produce big differences in drought resilience. This interpretation is consistent with the idea that landscape-level integrity provides a background condition — reducing human pressure, maintaining connectivity, and buffering edge effects — rather than directly controlling vegetation physiology during drought.

Despite its low direct SHAP importance, FLII should not be dismissed as unimportant. A recent global study found that forest fragmentation is associated with reduced drought resilience across multiple biomes, with stronger effects in tropical and temperate forests (Su et al., 2025). The fact that FLII did not emerge as a strong direct predictor here does not contradict this finding. Instead, it suggests that the pathway from landscape integrity to coarse-pixel-level drought resilience may be indirect, operating through mechanisms such as microclimate modification, reduced edge exposure, or maintenance of species pools, rather than through a direct effect on SIF-based resilience metrics.

Together, these results indicate that species-level and landscape-level forest integrity represent different dimensions of forest health. Tree species diversity showed a clearer direct relationship with pixel-level drought resilience, while FLII may operate through spatial and ecological

pathways that are less visible in a coarse pixel-level modelling framework. This distinction matters for forest management and conservation. Protecting landscape-level integrity — by reducing fragmentation, maintaining connectivity, and limiting human pressure — may support drought resilience through mechanisms that complement the species-level effects captured by tree species diversity. Future studies using multi-scale modelling approaches or landscape-level resilience metrics may be better suited to quantify the full contribution of FLII to ecosystem resilience.

5.5 Environmental context modifies the role of forest integrity

The SHAP interaction analysis showed that the effects of tree species diversity on drought resilience were not constant across environmental gradients but were modified by temperature, precipitation, and forest structure. This finding adds an important dimension to the interpretation of species-level forest integrity: its contribution to resistance and recovery depends on the climatic and structural context in which forests occur.

The interaction between tree species diversity and mean annual temperature was particularly informative. In terms of resistance, this interaction was negative, indicating that the positive effect of species diversity on resistance was weaker in warmer forests than in cooler forests. One possible explanation is that in warm environments, drought stress is often compounded by high evaporative demand (Allen et al., 2010; Anderegg et al., 2018). Under such conditions, even diverse communities may struggle to maintain aggregate function because the physiological limits imposed by heat and atmospheric dryness reduce the effectiveness of niche complementarity. In cooler environments, where thermal stress is lower and evaporative demand is more moderate, the complementary resource-use strategies present in diverse forests may have greater room to operate.

For recovery, the same interaction showed the opposite direction: the negative main effect of tree species diversity on recovery was partially offset under warmer conditions. This does not mean that warmer temperatures reversed the diversity–recovery relationship — rather, the magnitude of the negative association was smaller in warm forests than in cool forests. One interpretation is that in warm environments, favourable post-drought growing conditions, including longer growing seasons and higher energy availability, may allow even species-rich forests to show some degree of functional return after drought. In cooler environments, where the growing season is shorter and energy-limited, the slow recovery characteristic of diverse forests may be more pronounced.

The interaction between tree species diversity and mean annual precipitation showed a different pattern. In terms of resistance, precipitation appeared to strengthen the positive effect of diversity, especially at intermediate and high levels of diversity. This is consistent with the idea that water availability supports the complementary water-use strategies present in diverse forests. In very dry conditions, all species may be water-limited regardless of their functional diversity, reducing the additional benefit of having multiple strategies. In moderately wet conditions, differences in rooting depth, water-use efficiency, and stomatal regulation among species may become more effective. For recovery, the interaction with precipitation was weak, suggesting that moisture conditions had a less consistent modifying effect on the diversity–recovery relationship.

Tree cover also modified the effect of tree species diversity, particularly for recovery. High tree cover combined with high species diversity was associated with a positive interaction for recovery, suggesting that the negative effect of diversity on recovery was partially reduced in forests with dense canopy cover. This may reflect the role of canopy structure in buffering post-drought microclimate conditions. Dense canopies can moderate temperature extremes and reduce soil moisture loss, creating conditions that facilitate recovery even in species-rich communities that might otherwise recover slowly.

These interaction patterns have two broader implications. First, they reinforce the finding that resistance and recovery are shaped by different ecological processes. The same environmental gradient — temperature — modified the diversity effect in opposite directions for resistance and recovery, further supporting the interpretation that these two dimensions cannot be treated as interchangeable. Second, they indicate that the role of forest integrity in drought resilience is not fixed but varies with the environmental background. Global estimates of diversity–resilience relationships may therefore mask substantial regional variation, and management strategies aimed at enhancing drought resilience through biodiversity conservation should consider the local environmental context, rather than assuming a uniform positive effect of diversity across all conditions.

It should be noted that the interaction effects identified here represent marginal modifications to the main SHAP contributions, not reversals of the overall spatial patterns described in Sections 4.2 and 4.7. For example, although the positive interaction between tree species diversity and temperature partially offset the negative main effect of diversity on recovery in warm regions, the overall predicted recovery in tropical forests remained low because the main

effects of temperature, tree cover, and diversity were all negative in these regions. The interaction results should therefore be interpreted as fine-scale modulations within the broader spatial patterns, not as contradictions to them.

5.6 Limitations and future directions

Several limitations of this study should be considered when interpreting the results.

First, the analysis is based on correlative modelling and cannot establish causal relationships. The Random Forest models identified statistical associations between predictors and drought resilience metrics, and the SHAP analysis quantified the marginal contribution of each predictor within the fitted models. However, these associations may be influenced by unmeasured confounding variables or by correlations among predictors that cannot be fully disentangled by the modelling approach. For example, the strong association between tree species diversity and drought resistance may partly reflect the climatic and biogeographic conditions under which high-diversity forests occur, rather than a direct causal effect of species richness on ecosystem function. Experimental or quasi-experimental approaches, such as comparisons across biodiversity gradients within similar climate zones, would provide stronger evidence for causality.

Second, the drought resilience metrics used in this study were derived from satellite-based SIF anomalies at a monthly temporal resolution. SIF captures canopy-level photosynthetic activity and is well suited for detecting vegetation responses to drought at the global scale, but it may not fully represent all dimensions of ecosystem drought response, such as changes in belowground processes, tree mortality, or shifts in species composition. The monthly resolution may also miss short-lived drought events or fail to capture rapid recovery dynamics on sub-monthly timescales. Future studies using higher-temporal-resolution data or complementary remote sensing indicators, such as vegetation optical depth or solar-induced fluorescence, at finer temporal scales may capture additional aspects of drought resilience.

Third, the analysis used pixel-level medians at 0.05° resolution, which limits its ability to resolve event-level and fine-scale heterogeneity. Resistance and recovery were summarised as pixel-level medians across multiple drought events; this aggregation was necessary to link event-level dynamics to spatial predictors, but lost information about how individual events differed in severity, duration, or timing. Two forests with identical median resistance may differ substantially in their response to specific droughts, and the low predictive performance of the trade-off model (validation $R^2 = 0.043$) may partly reflect this loss of event-level information.

At the same time, the 0.05° pixel size (approximately 5.5 km at the equator) cannot capture fine-scale heterogeneity in forest structure, topography, or microclimate that can influence local drought responses, including at forest edges, in riparian corridors, and under topographic sheltering. The effects of landscape-level integrity in particular may be better captured at finer spatial units or through multi-scale modelling approaches, as discussed in Section 5.4.

Fourth, the predictor set, while comprehensive, does not include all potentially relevant variables. Root depth, soil water holding capacity, stand age, management history, and species-level functional trait composition were not available at the global scale and resolution required for this analysis. These variables may influence drought resilience through pathways that are not captured by the current predictors. In particular, the weak direct effect of FLII may be partly attributable to the absence of fine-scale variables that mediate the relationship between landscape integrity and coarse pixel-level drought resilience.

Despite these limitations, this study provides a global perspective on the relationship between forest integrity and drought resilience, complementing existing regional and experimental studies. Several directions for future research emerge from the findings. First, multi-scale analyses linking landscape-level integrity metrics to drought resilience across multiple spatial resolutions could help clarify the roles of FLII and other landscape indicators. Second, incorporating species-level functional trait data — such as hydraulic traits, wood density distributions, or rooting depth profiles — could provide more mechanistic insight into why species diversity affects resistance and recovery in opposite directions. Third, analysing the interaction between forest integrity and drought characteristics at the event level, rather than using pixel-level summaries, could improve understanding of the resistance–recovery trade-off. Finally, extending the analysis to include post-2022 data would allow the framework developed here to be tested against more recent drought events, including those associated with ongoing climate warming.

6. Conclusion

This thesis assessed how landscape-level forest integrity (FLII) and species-level forest integrity (tree species diversity) are associated with drought resistance and recovery in global stable forests. Using 22 years of GOSIF SIF data, SPEI-3-based drought events, and machine-learning models controlling for climate, soil, topography, and forest structure, four main conclusions emerge.

First, resistance and recovery represent different dimensions of drought resilience. Tropical and subtropical forests generally showed high resistance but low recovery, whereas boreal and temperate forests showed the opposite. A negative event-level correlation between resistance and recovery was found in 72.98% of the modelling sample, confirming that the resistance–recovery trade-off is a widespread feature of global forests.

Second, tree species diversity was positively associated with resistance but negatively associated with recovery. The hypothesis that diversity would improve both dimensions was therefore only partially supported, likely reflecting baseline ceiling effects in high-biomass forests and trade-offs between drought-tolerant and fast-recovering strategies.

Third, FLII showed a weaker direct contribution than species diversity. This does not imply that landscape integrity is ecologically unimportant, but rather that its effects may operate at spatial scales beyond the coarse pixel-level resolution of the framework used here.

Fourth, the effects of forest integrity depended on environmental context, particularly temperature. Global mean estimates of diversity–resilience relationships therefore mask substantial regional variation.

Together, these findings show that forest integrity cannot be represented by a single dimension and that resistance and recovery cannot be treated as interchangeable components of forest drought resilience. Distinguishing these dimensions and their context-dependent nature will become increasingly important for forest conservation and nature-based climate solutions under intensifying drought regimes.

References

Allen, C. D., Macalady, A. K., Chenchouni, H., Bachelet, D., McDowell, N., Vennetier, M., Kitzberger, T., Rigling, A., Breshears, D. D., Hogg, E. H., Gonzalez, P., Fensham, R., Zhang, Z., Castro, J., Demidova, N., Lim, J. H., Allard, G., Running, S. W., Semerci, A., & Cobb, N. (2010). A global overview of drought and heat-induced tree mortality reveals emerging climate change risks for forests. *Forest Ecology and Management*, *259*(4), 660–684. https://doi.org/10.1016/j.foreco.2009.09.001

Amatulli, G., Domisch, S., Tuanmu, M.-N., Parmentier, B., Ranipeta, A., Malczyk, J., & Jetz, W. (2018). A suite of global, cross-scale topographic variables for environmental and biodiversity modeling. *Scientific Data*, *5*, 180040. https://doi.org/10.1038/sdata.2018.40

Anderegg, W. R. L., Konings, A. G., Trugman, A. T., Yu, K., Bowling, D. R., Gabbitas, R., Karp, D. S., Pacala, S., Sperry, J. S., Sulman, B. N., & Zenes, N. (2018). Hydraulic diversity of forests regulates ecosystem resilience during drought. *Nature*, *561*(7724), 538–541. https://doi.org/10.1038/s41586-018-0539-7

Bai, Y., & Tang, Z. (2024). Enhanced effects of species richness on resistance and resilience of global tree growth to prolonged drought. *Proceedings of the National Academy of Sciences*, *121*(39), e2410467121. https://doi.org/10.1073/pnas.2410467121

Banbury Morgan, R., & Jucker, T. (2025). A unifying framework for understanding how edge effects reshape the structure, composition and function of forests. *New Phytologist*, *248*(2), 529–541. https://doi.org/10.1111/nph.70457

Behera, A. D., Mishra, V., Pradhan, P., Sharma, A., & Joshi, M. (2025). Solar-induced chlorophyll fluorescence yield holds the potential for drought early warning. *Geophysical Research Letters*, *52*(4), e2024GL113419. https://doi.org/10.1029/2024GL113419

De Frenne, P., Zellweger, F., Rodríguez-Sánchez, F., Scheffers, B. R., Hylander, K., Luoto, M., Vellend, M., Verheyen, K., & Lenoir, J. (2019). Global buffering of temperatures under forest canopies. *Nature Ecology & Evolution*, *3*(5), 744–749. https://doi.org/10.1038/s41559-019-0842-1

De Keersmaecker, W., Lhermitte, S., Tits, L., Honnay, O., Somers, B., & Coppin, P. (2015). A model quantifying global vegetation resistance and resilience to short-term climate anomalies and their relationship with vegetation cover. *Global Ecology and Biogeography*, *24*(5), 539–548. https://doi.org/10.1111/geb.12279

FAO/IIASA/ISRIC/ISS-CAS/JRC. (2012). *Harmonized World Soil Database (version 1.2)*. FAO, Rome, Italy and IIASA, Laxenburg, Austria.

Forzieri, G., Dakos, V., McDowell, N. G., Ramdane, A., & Cescatti, A. (2022). Emerging signals of declining forest resilience under climate change. *Nature*, *608*(7923), 534–539. https://doi.org/10.1038/s41586-022-04959-9

Grantham, H. S., Duncan, A., Evans, T. D., Jones, K. R., Beyer, H. L., Schuster, R., Walston, J., Ray, J. C., Robinson, J. G., Callow, M., Clements, T., Costa, H. M., DeGemmis, A., Elsen, P. R., Ervin, J., Franco, P., Goldman, E., Goetz, S., Hansen, A., … Watson, J. E. M. (2020). Anthropogenic modification of forests means only 40% of remaining forests have high ecosystem integrity. *Nature Communications*, *11*, 5978. https://doi.org/10.1038/s41467-020-19493-3

Grossiord, C., Granier, A., Ratcliffe, S., Bouriaud, O., Bruelheide, H., Chećko, E., Forrester, D. I., Dawud, S. M., Finér, L., Pollastrini, M., Scherer-Lorenzen, M., Valladares, F., Bonal, D., & Gessler, A. (2014). Tree diversity does not always improve resistance of forest ecosystems to drought. *Proceedings of the National Academy of Sciences*, *111*(41), 14812–14815. https://doi.org/10.1073/pnas.1411970111

Haddad, N. M., Brudvig, L. A., Clobert, J., Davies, K. F., Gonzalez, A., Holt, R. D., Lovejoy, T. E., Sexton, J. O., Austin, M. P., Collins, C. D., Cook, W. M., Damschen, E. I., Ewers, R. M., Foster, B. L., Jenkins, C. N., King, A. J., Laurance, W. F., Levey, D. J., Margules, C. R., … Townshend, J. R. (2015). Habitat fragmentation and its lasting impact on Earth's ecosystems. *Science Advances*, *1*(2), e1500052. https://doi.org/10.1126/sciadv.1500052

Hansen, M., & Song, X.-P. (2018). *Vegetation Continuous Fields (VCF) Yearly Global 0.05 Deg* [Data set]. NASA EOSDIS Land Processes DAAC. https://doi.org/10.5067/MEASURES/VCF/VCF5KYR.001

Hillebrand, H., Langenheder, S., Lebret, K., Lindström, E., Östman, Ö., & Striebel, M. (2018). Decomposing multiple dimensions of stability in global change experiments. *Ecology Letters*, *21*(1), 21–30. https://doi.org/10.1111/ele.12867

Hodgson, D., McDonald, J. L., & Hosken, D. J. (2015). What do you mean, 'resilient'? *Trends in Ecology & Evolution*, *30*(9), 503–506. https://doi.org/10.1016/j.tree.2015.06.010

Hubau, W., Lewis, S. L., Phillips, O. L., Affum-Baffoe, K., Beeckman, H., Cuní-Sanchez, A., Daniels, A. K., Ewango, C. E. N., Fauset, S., Mukinzi, J. M., Sheil, D., Sonké, B., Sullivan, M. J. P., Sunderland, T. C. H., Taedoumg, H., Thomas, S. C., White, L. J. T., Abernethy, K. A., Adu-Bredu, S., … Zemagho, L. (2020). Asynchronous carbon sink saturation in African and Amazonian tropical forests. *Nature*, *579*(7797), 80–87. https://doi.org/10.1038/s41586-020-2035-0

Ingrisch, J., & Bahn, M. (2018). Towards a comparable quantification of resilience. *Trends in Ecology & Evolution*, *33*(4), 251–259. https://doi.org/10.1016/j.tree.2018.01.013

Isbell, F., Craven, D., Connolly, J., Loreau, M., Schmid, B., Beierkuhnlein, C., Bezemer, T. M., Bonin, C., Bruelheide, H., de Luca, E., Ebeling, A., Griffin, J. N., Guo, Q., Hautier, Y., Hector, A., Jentsch, A., Kreyling, J., Lanta, V., Manning, P., … Eisenhauer, N. (2015). Biodiversity increases the resistance of ecosystem productivity to climate extremes. *Nature*, *526*(7574), 574–577. https://doi.org/10.1038/nature15374

Koelemeijer, I. A., Ehrlén, J., Jönsson, M., De Frenne, P., Berg, M., Andersson, J., Weibull, B., & Hylander, K. (2023). Forest edge effects on moss growth are amplified by drought. *Ecological Applications*, *33*(4), e2851. https://doi.org/10.1002/eap.2851

Li, X., & Xiao, J. (2019). A global, 0.05-degree product of solar-induced chlorophyll fluorescence derived from OCO-2, MODIS, and reanalysis data. *Remote Sensing*, *11*(5), 517. https://doi.org/10.3390/rs11050517

Liang, J., Crowther, T. W., Picard, N., Wiser, S., Zhou, M., Alberti, G., Schulze, E.-D., McGuire, A. D., Bozzato, F., Pretzsch, H., de-Miguel, S., Paquette, A., Hérault, B., Scherer-Lorenzen, M., Barrett, C. B., Glick, H. B., Hengeveld, G. M., Nabuurs, G.-J., Pfautsch, S., … Reich, P. B. (2022). Co-limitation towards lower latitudes shapes global forest diversity gradients. *Nature Ecology & Evolution*, *6*(10), 1423–1437. https://doi.org/10.1038/s41559-022-01831-x

Liu, D., Wang, T., Peñuelas, J., & Piao, S. (2022). Drought resistance enhanced by tree species diversity in global forests. *Nature Geoscience*, *15*(10), 800–804. https://doi.org/10.1038/s41561-022-01026-w

Lloret, F., Keeling, E. G., & Sala, A. (2011). Components of tree resilience: Effects of successive low-growth episodes in old ponderosa pine forests. *Oikos*, *120*(12), 1909–1920. https://doi.org/10.1111/j.1600-0706.2011.19372.x

Lundberg, S. M., Erion, G., Chen, H., DeGrain, A., Prutkin, J. M., Nair, B., Katz, R., Himmelfarb, J., Bansal, N., & Lee, S.-I. (2020). From local explanations to global understanding with explainable AI for trees. *Nature Machine Intelligence*, *2*(1), 56–67. https://doi.org/10.1038/s42256-019-0138-9

Muñoz-Sabater, J., Dutra, E., Agustí-Panareda, A., Albergel, C., Arduini, G., Balsamo, G., Boussetta, S., Choulga, M., Harrigan, S., Hersbach, H., Martens, B., Miralles, D. G., Piles, M., Rodríguez-Fernández, N. J., Zsoter, E., Buontempo, C., & Thépaut, J.-N. (2021). ERA5-Land: A state-of-the-art global reanalysis dataset for land applications. *Earth System Science Data*, *13*(9), 4349–4383. https://doi.org/10.5194/essd-13-4349-2021

Pimm, S. L. (1984). The complexity and stability of ecosystems. *Nature*, *307*(5949), 321–326. https://doi.org/10.1038/307321a0

Runge, K., Smith, T., Boers, N., & Thonicke, K. (2025). Monitoring terrestrial ecosystem resilience using Earth observation data: Identifying consensus and limitations across metrics. *Global Change Biology*, *31*(3), e70115. https://doi.org/10.1111/gcb.70115

Schwalm, C. R., Anderegg, W. R. L., Michalak, A. M., Fisher, J. B., Biondi, F., Koch, G., Litvak, M., Ogle, K., Shaw, J. D., Wolf, A., Huntzinger, D. N., Schaefer, K., Cook, R., Wei, Y., Fang, Y., Hayes, D., Huang, M., Jain, A., & Tian, H. (2017). Global patterns of drought recovery. *Nature*, *548*(7666), 202–205. https://doi.org/10.1038/nature23021

Song, X.-P., Hansen, M. C., Stehman, S. V., Potapov, P. V., Tyukavina, A., Vermote, E. F., & Townshend, J. R. (2018). Global land change from 1982 to 2016. *Nature, 560*, 639–643. https://doi.org/10.1038/s41586-018-0411-9

Sturm, J., Santos, M. J., Schmid, B., & Damm, A. (2022). Satellite data reveal differential responses of Swiss forests to unprecedented 2018 drought. *Global Change Biology*, *28*(9), 2956–2978. https://doi.org/10.1111/gcb.16136

Su, Y., Zhang, C., Cescatti, A., Yu, K., Ciais, P., Smith, T., Shang, J., Carnicer, J., Liu, J., Chen, J. M., Green, J. K., Wu, J., Ponce-Campos, G. E., Zhang, Y., Zuo, Z., Liao, J., Lafortezza, R., Yan, K., Yang, X., … Zhou, W. (2025). Pervasive but biome-dependent relationship between fragmentation and resilience in forests. *Nature Ecology & Evolution*, *9*(9), 1670–1684. https://doi.org/10.1038/s41559-025-02776-7

Sun, Y., Fu, R., Dickinson, R., Joiner, J., Frankenberg, C., Gu, L., Xia, Y., & Fernando, N. (2015). Drought onset mechanisms revealed by satellite solar-induced chlorophyll fluorescence: Insights from two contrasting extreme events. *Journal of Geophysical Research: Biogeosciences*, *120*(11), 2427–2440. https://doi.org/10.1002/2015JG003150

Vicente-Serrano, S. M., Beguería, S., & López-Moreno, J. I. (2010). A multiscalar drought index sensitive to global warming: The standardized precipitation evapotranspiration index. *Journal of Climate*, *23*(7), 1696–1718. https://doi.org/10.1175/2009JCLI2909.1

Watson, J. E. M., Evans, T., Venter, O., Williams, B., Tulloch, A., Stewart, C., Thompson, I., Ray, J. C., Murray, K., Salazar, A., McAlpine, C., Potapov, P., Walston, J., Robinson, J. G., Painter, M., Wilkie, D., Filardi, C., Laurance, W. F., Houghton, R. A., … Lindenmayer, D. (2018). The exceptional value of intact forest ecosystems. *Nature Ecology & Evolution*, *2*(4), 599–610. https://doi.org/10.1038/s41559-018-0490-x

Wu, X., & Liu, Y. (2025). Altitude weakens the drought resistance–resilience tradeoff across northern ecosystems. *Agricultural and Forest Meteorology*, *372*, 110758. https://doi.org/10.1016/j.agrformet.2025.110758

Xu, C., McDowell, N. G., Fisher, R. A., Wei, L., Sevanto, S., Christoffersen, B. O., Weng, E., & Middleton, R. S. (2019). Increasing impacts of extreme droughts on vegetation productivity under climate change. *Nature Climate Change*, *9*(12), 948–953. https://doi.org/10.1038/s41558-019-0630-6

Yao, Y., Liu, Y., Song, J., Tao, S., Li, Y., Wu, T., Wang, Y., Wang, S., & Fu, B. (2024). Declining tradeoff between resistance and resilience of ecosystems to drought. *Earth's Future*, *12*(5), e2024EF004665. https://doi.org/10.1029/2024EF004665

AI declaration

AI assistance was used to improve texts and identify code errors. All analysis, editorial judgement, and conclusions are the author's own.